Alberti et al. Journal of Palaeogeography (2021) 10:24
https://doi.org/10.1186/s42501-021-00103-2

Journal of Palaeogeography

ORIGINAL ARTICLE Open Access

First record of stable isotopes ($\delta^{13}C$, $\delta^{18}O$) and element ratios (Mg/Ca, Sr/Ca) of Middle to Late Jurassic belemnites from the Indian Himalayas and their potential for palaeoenvironmental reconstructions

Matthias Alberti[1*], Franz T. Fürsich[2], Dhirendra K. Pandey[3,4], Nils Andersen[5], Dieter Garbe-Schönberg[6], Suraj Bhosale[4], Ketan Chaskar[4] and Jörg M. Habermann[2]

Abstract

Middle to Late Jurassic belemnites from the Spiti and Zanskar valleys in the Indian Himalayas were used for stable isotope ($\delta^{13}C$, $\delta^{18}O$) and element (Mg/Ca, Sr/Ca) analyses. Although the Himalayan orogeny deformed and altered a large portion of the collected fossils, cathodoluminescence and scanning electron microscopy in combination with analyses of iron and manganese contents allowed the identification of belemnites believed to still retain their original chemical composition. Results indicate a long-term temperature decrease from the Middle Callovian–Oxfordian to the Tithonian, which is proposed to have been caused by a concomitant drift of eastern Gondwana into higher palaeolatitudes. Reconstructed absolute temperatures depend on the used equation and assumed $\delta^{18}O$ value of seawater, but most likely varied between 17.6 °C to 27.6 °C in the Kimmeridgian and Tithonian with average values between 22 °C to 24 °C. This way, temperatures were similar to slightly warmer than today at comparable latitudes. The reconstruction of absolute temperatures for the Middle Callovian–Oxfordian was hindered by a larger number of poorly preserved belemnites representing this time interval.

Keywords: Jurassic, Palaeoclimate, Water temperature, Spiti, Zanskar, India, Tethyan Himalaya, Eastern Gondwana

1 Introduction

Since many decades, stable oxygen isotope ($\delta^{18}O$) analyses of fossil shells have been used to reconstruct the temperature development throughout Earth's history, including the Jurassic period (e.g. Epstein et al. 1951; Urey et al. 1951; Bowen 1963; Stevens and Clayton 1971). The temporal resolution of these palaeoenvironmental reconstructions has increased considerably, but the available data are still dominated by results from European localities (e.g. Korte et al. 2015; Martinez and Dera 2015). Originally, these European $\delta^{18}O$ records seemed to reflect a long-term warming throughout the Late Jurassic (compare Dera et al. 2011), but it was not clear whether this represented global or local changes due to a scarcity of data from other regions. In the meantime, clumped isotope analyses suggested that Late Jurassic temperature fluctuations reconstructed for European material might be overestimated (e.g. Wierzbowski et al. 2018). Consequently , it seems worthwhile to focus more energy on yet understudied regions outside Europe, such as parts of Gondwana, to identify truly global climate patterns of the past. Although data are still sparse, recent studies

* Correspondence: matthias_alberti@nju.edu.cn
[1]State Key Laboratory for Mineral Deposits Research, School of Earth Sciences and Engineering, Centre for Research and Education on Biological Evolution and Environment and Frontiers Science Center for Critical Earth Material Cycling, Nanjing University, Nanjing 210023, Jiangsu Province, China
Full list of author information is available at the end of the article

© The Author(s). 2021 **Open Access** This article is licensed under a Creative Commons Attribution 4.0 International License, which permits use, sharing, adaptation, distribution and reproduction in any medium or format, as long as you give appropriate credit to the original author(s) and the source, provide a link to the Creative Commons licence, and indicate if changes were made. The images or other third party material in this article are included in the article's Creative Commons licence, unless indicated otherwise in a credit line to the material. If material is not included in the article's Creative Commons licence and your intended use is not permitted by statutory regulation or exceeds the permitted use, you will need to obtain permission directly from the copyright holder. To view a copy of this licence, visit http://creativecommons.org/licenses/by/4.0/.

suggest that low-latitudinal regions of western Gondwana (e.g. Egypt, Algeria) showed comparatively stable temperatures throughout the Middle and Late Jurassic, while eastern Gondwana experienced a concurrent temperature decrease (Fürsich et al. 2005; Alberti et al. 2017, 2019, 2020a; Sadji et al. 2021). The latter has been found in fossil records from Madagascar and western India (Kachchh), but data are still sparse particularly in the Late Jurassic. The present study therefore uses fossil material from the Indian Himalayas with Callovian to Tithonian ages to examine its potential for palaeoenvironmental reconstructions.

2 Geological overview

In the Himalayas, marine sedimentary rocks with a Jurassic age (Tethyan strata; Pathak 2007; Pandey et al. 2013) form a belt stretching from northern Pakistan through India and Nepal until southwestern China. Three regions within the Indian part of this belt are described in greater detail in the literature: Zanskar, Spiti, and Kumaon (e.g. Blanford 1864; Stoliczka 1865; Uhlig 1903; Holdhaus 1912; Brookfield and Westermann 1982; Krishna et al. 1982; Baud et al. 1984; Jain et al. 1984; Jadoul et al. 1985, 1990; Gaetani et al. 1986; Oloriz and Tintori 1991; Pathak 1993, 2007; Garzanti et al. 1995; Tiwari et al. 1996; Bhargava and Bassi 1998; Vijaya 2002; Bertle and Suttner 2005, 2021; Pandey et al. 2013). While the Kumaon outcrops (also referred to in the literature as Malla Johar, Niti, and Laptal) are situated in a restricted border-region and were not accessible during the present project, sections within the Spiti and Zanskar valleys were measured and sampled (Fig. 1).

In general, the examined successions of the Spiti and Zanskar valleys start with more than 600 m of well-cemented, thick-bedded limestones which constitute the Para and Tagling formations of the Kioto Group with a Triassic to Middle Jurassic age (Figs. 2, 3a, b; e.g. Jadoul et al. 1985; Garzanti et al. 1995; Bhargava 2008). These rocks formed in a comparatively shallow setting exemplified by common cross-bedding. Many horizons contain shell fragments, but due to their strong cementation, it is often impossible to collect complete, identifiable fossils. Consequently, dating by index fossils is complicated and the exact position of the Triassic–Jurassic boundary is unknown. The strata show an increase in siliciclastic content towards the top, the latter being

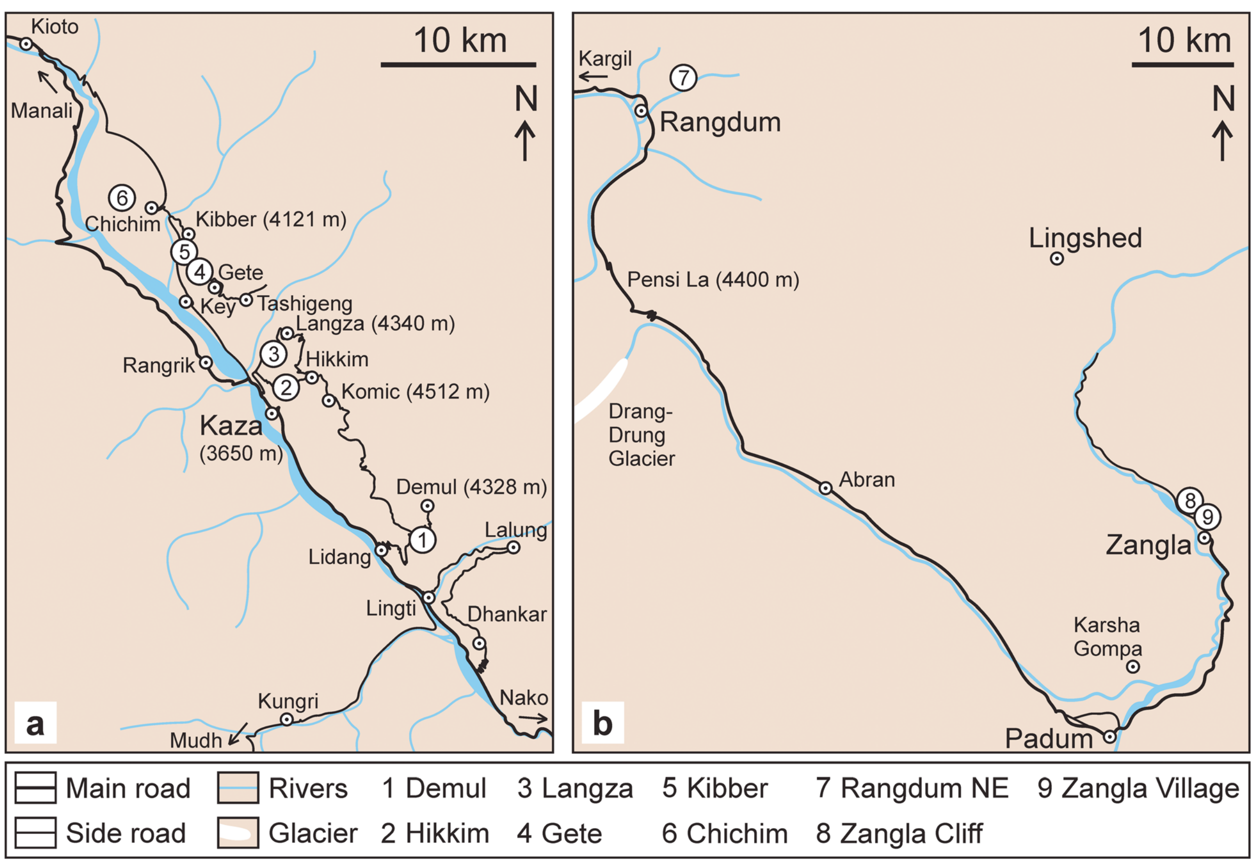

Fig. 1 **a** Road map of the Spiti Valley in northeastern Himachal Pradesh showing the location of the studied sections; **b** Road map of the Zanskar Valley in northwestern Ladakh showing the location of the studied sections

Lithostratigraphy			Thickness	Lithology	Age
Lagudarsi Group	Giumal Formation		~400 m	- Glauconitic sandstones and siltstones - Few bivalves	Albian –Berriasian
Lagudarsi Group	Spiti Shale Fm	Upper member (Lochambel Beds)	<300 m	- Shaly argillaceous silt and common thin sandstone beds - Fossils comparatively rare	?Berriasian –Early Tithonian
Lagudarsi Group	Spiti Shale Fm	Middle member (Chidamu Beds)	<300 m	- Shaly argillaceous silt with abundant concretions and occasional thin sandstone intercalations - Common ammonites	Early Tithonian –Kimmeridgian
Lagudarsi Group	Spiti Shale Fm	Lower member (*B. gerardi* Beds)	<300 m	- Shaly argillaceous silt - Abundant belemnites and common bivalves	Late Oxfordian –Middle Callovian
Kioto Gr	Ferruginous Oolite Fm		0–20 m	- Cross-bedded sandstones, siltstones, and limestones - Some beds with ferruginous ooids - occasional belemnite concentrations	Early Callovian –Early Bathonian
Kioto Gr	Para and Tagling Fms		~600 m	- Well-cemented, thick-bedded limestones - Hardgrounds with encrusting oysters near top - Common shell fragments	Middle Jurassic –Triassic

Fig. 2 Summary on the different lithostratigraphic units in the Spiti and Zanskar valleys with a Jurassic to Early Cretaceous age (information combined from Krishna et al. 1982; Cariou et al. 1996; Pathak 1997, 2007; Bertle and Suttner 2005, 2021; Bhargava 2008; Lukeneder et al. 2013; Pandey et al. 2013). Note that thicknesses and lithologies can change considerably between localities

most likely Bathonian in age (e.g. Oloriz and Tintori 1991). Near its top there are a number of hardgrounds characterized by encrusting oysters and bivalve borings, which indicate phases of sediment starvation and sedimentary gaps (Fig. 3c).

The following unit is the Ferruginous Oolite Formation, which shows a variable lithology with several cross-bedded sandstones, siltstones, and limestones with ferruginous ooids. Its rocks are softer and previous authors have described Bathonian and Callovian ammonites from this unit (e.g. Krishna et al. 1982; Jadoul et al. 1985; Cariou and Enay 1999). The Ferruginous Oolite Formation changes in thickness and lithology laterally. While it is relatively well exposed in the Zanskar region with a thickness of more than 20 m (also compare Jadoul et al. 1985), it is less conspicuous in the Spiti Valley (see Fig. 3b, h, i; compare Gupta and Kumar 1975).

The Ferruginous Oolite Formation is overlain by the Spiti Shale Formation of the Lagudarsi Group (Fig. 2), which is dominated by blackish-grey silty clay and ferruginous concretions and represents a deeper-water environment, generally below wave base. The soft rocks locally contain abundant fossils, including ammonites and belemnites (predominantly Belemnopseidae, such as the abundant *Belemnopsis grantianus* = *B. gerardi*; Cariou et al. 1996). Benthic groups are commonly restricted to individual horizons and include bivalves, few brachiopods, and rare gastropods. Changes in the benthic communities indicate occasional anoxic to dysoxic conditions at the sea floor (e.g. Baud et al. 1984). The Spiti Shale Formation is generally subdivided into three members, which can be separated by comparatively minor differences such as the abundance of concretions and changes in fossil content (Figs. 2, 3d, f). Due to the formation's soft nature, good outcrops are rare and tectonic faulting and folding are prominent. This complicates the measurement of detailed continuous sections and different thicknesses have been reported for the unit in the Spiti Valley by previous authors, e.g., 300 m by Pathak (2007) and 92 m by Pandey et al. (2013). Towards its top, more and more sandstone beds produce a gradual lithological change to the overlying Giumal Formation (Figs. 2, 3g). In contrast, outcrops in the Zanskar range exhibit only 20–60 m of Spiti Shale Formation with an apparent increase in thickness from west to east (Jadoul et al. 1985; Gaetani et al. 1986; Oloriz and Tintori 1991). Previous authors suggested a fault contact with the overlying Cretaceous sandstones of the Giumal Formation in Zanskar (compare Fig. 3b and Fig. 3h; Jadoul et al. 1985; Oloriz and Tintori 1991).

Geographically, the Spiti Valley with its administrative capital Kaza is situated in northeastern Himachal Pradesh (Fig. 1a). The eastern/northern side of the valley is formed by a steep cliff consisting of the massive limestones of the Para and Tagling formations (Fig. 3a). The lithological change to the much softer Spiti Shale Formation leads to a dramatic change in landscape, with the latter forming plateaus and gentle slopes and constituting seasonal pastures for livestock (Fig. 3b). In the present study, fossils for geochemical analyses were collected at fresh outcrops near the villages of Demul, Hikkim, Langza, Gete, Kibber, and Chichim (Fig. 1a). All of these sections are located at altitudes above 4000 m and can be reached easily via car from Kaza. Geographic coordinates for the individual sample locations are given together with analytical results (in Table 2 below).

The Zanskar Valley with its administrative capital Padum is situated in northwestern Ladakh (Fig. 1b). The

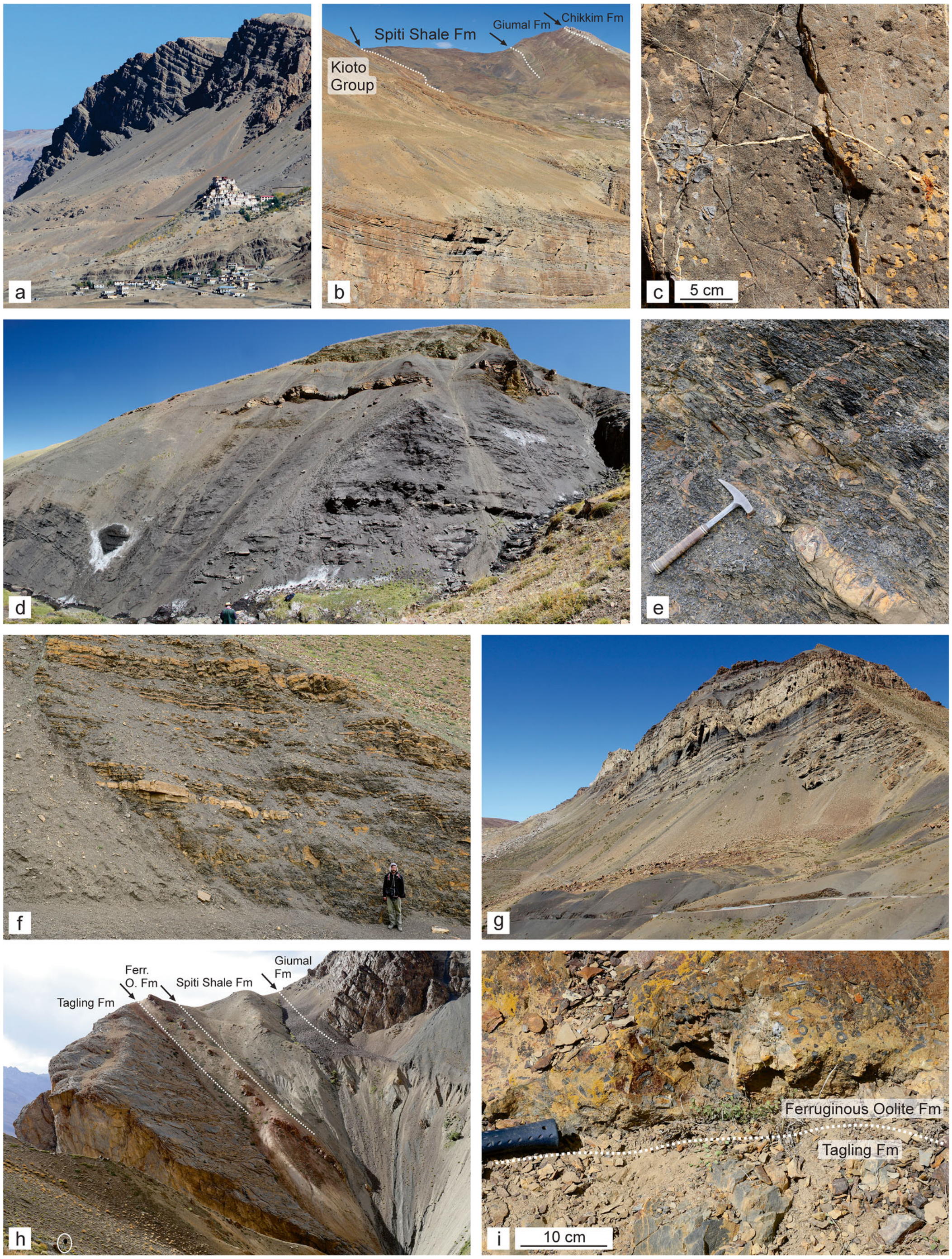

Fig. 3 Field photographs from the Spiti (**a** – **g**) and Zanskar valleys (**h**, **i**). **a** The Para and Tagling formations of the Kioto Group form a massive cliff along the eastern/northern side of the Spiti Valley (at Key Monastery); **b** Due to its softer nature, the Spiti Shale Formation forms a plateau on top of the harder rocks of the Kioto Group (view from Kibber towards Chichim); **c** Hardgrounds at the top of the Tagling Formation are characterized by encrusting oysters and bivalve borings (near Chichim); **d** Section through the Lower and parts of the Middle member of the Spiti Shale Formation (near Langza), note person for scale; **e** Outcrop photo of the Middle member of the Spiti Shale Formation with bands of ferruginous concretions (near Hikkim), note hammer for scale (ca. 32 cm in length); **f** Section through the Upper member of the Spiti Shale Formation (near Chichim), note person for scale; **g** A gradually increasing number of sandstone beds indicate the border between the Spiti Shale Formation and the Giumal Formation (near Demul); **h** The section at Zangla Cliff is characterized by a relatively thick Ferruginous Oolite Formation and a comparatively thin Spiti Shale Formation, note person for scale; **i** Close-up view of the boundary between the Tagling Formation and the Ferruginous Oolite Formation at Rangdum NE. Note the abundant belemnites concentrated at the base of the Ferruginous Oolite Formation

Jurassic strata are exposed along a belt north of the actual valley, forming part of the Zanskar range. In this region, the Ferruginous Oolite Formation is much more conspicuous compared to the Spiti Valley (Fig. 3h, i). Unfortunately, the Jurassic strata in the Zanskar Valley contain only few fossils. Sections were measured and belemnites for geochemical analyses were collected at the hill slope of a river valley 5.5 km northeast of Rangdum Monastery, above a cliff reachable through a narrow gorge 3.5 km north of Zangla, and at the hill side directly north of Zangla Village (Fig. 1b). Further Jurassic outcrops in the region were described in literature near Lingshed Monastery (Oloriz and Tintori 1991), but these sections are only reachable on foot via several days of trekking and could not be accessed during the present study. Geographic coordinates of the individual sample locations are given together with analytical results below (also see Table 2).

3 Biostratigraphy

Dating of the Spiti Shale Formation is possible with the help of ammonites as guide fossils (e.g. Krishna 1983; Enay 2009; Pandey et al. 2013; compare Fig. 2). Cariou et al. (1996) recorded species of *Idiocycloceras*, *Kinkeliniceras*, *Hubertoceras*, *Obtusicostites*, *Grossouvria*, and *Macrocephalites* of an early Middle Callovian age from the base of the Lower member in the Spiti Valley. The authors collected most of these specimens from a single oolitic limestone bed and suggested the repeated occurrence of condensed beds or sedimentary gaps in the succession, which are, however, not visible in the monotonous sediments. Interestingly, most other authors have restricted the age of the basal Spiti Shale Formation to the Oxfordian (e.g. Krishna et al. 1982; Pathak 1997, 2007), based on records of mayaitids as well as *Prograyiceras* and perisphinctids (compare also Cariou et al. 1996; Enay 2009; Pandey et al. 2013). The occurrence of Callovian ammonites in the basal Spiti Shale Formation could not be confirmed during the present field surveys. While measuring the studied sections three specimens of *Epimayaites* were collected in the middle part of the Lower member, which would indicate an Oxfordian age (compare Alberti et al. 2015). Consequently, samples from the Lower member are considered here to be Middle Callovian–Oxfordian in age.

The lower part of the Middle member of the Spiti Shale Formation is characterized by the presence of *Pachysphinctes*, *Glochiceras*, and *Torquatisphinctes* and has been assigned to the Kimmeridgian by Pandey et al. (2013; also see Pathak 1997). The upper part of the Middle member is already Early Tithonian in age based on the presence of ammonites such as *Aulacosphinctoides*, *Virgatosphinctes*, and *Hybonoticeras* (Pathak 1997; Pandey et al. 2013). These earlier age assignments were supported in the present field surveys based on additional ammonite records. Consequently, fossils for geochemical analyses collected from the lower part of the Middle member were assigned to the Kimmeridgian.

The Upper member of the Spiti Shale Formation has been assigned to the late Early–Late Tithonian and partly Early Cretaceous (compare Krishna et al. 1982; Oloriz and Tintori 1991; Pathak 1997, 2007; Pandey et al. 2013). Ammonites are relatively common in these strata including Tithonian forms such as *Himalayites*, *Blanfordiceras*, *Uhligites*, and *Corongoceras*, and Early Cretaceous genera such as *Neocosmoceras* and *Spiticeras* (compare Krishna et al. 1982; Pathak 2007; Enay 2009; Pandey et al. 2013). Results of the present field surveys largely agree with these earlier assignments, which also allowed the dating of the collected belemnites to the Early and Late Tithonian.

4 Material and methods

The fossil material used in the present study was collected during two field surveys to the Spiti and Zanskar valleys in September 2016 and September 2018. In addition to the collection of samples for geochemical analyses, a considerable number of ammonites was retrieved and used for age assignments in combination with literature data (see above). The majority of the collected material constitutes Middle Callovian–Oxfordian to Tithonian belemnites (Belemnopseidae) from the Spiti Shale Formation, while oysters and fossils from the Bathonian to Callovian Tagling and Ferruginous Oolite formations were rare.

The collected fossils were prepared following standard methodology (compare Wierzbowski 2002, 2004; Alberti et al. 2012a; Danise et al. 2020). Sections of 5–10 mm thickness were cut in the laboratory and their surface was ground. Subsequently, all selected fossils were examined for signs of diagenetic alteration with a cold cathodoluminescence microscope at the GeoZentrum Nordbayern of the Friedrich-Alexander-Universität Erlangen-Nürnberg, Germany. Predominantly non-luminescent shell areas were selected for sampling, while luminescent (and therefore potentially altered) specimens were excluded from analysis or used only for comparison. Selected specimens were additionally examined using a scanning electron microscope at the Institut für Geowissenschaften of the Christian-Albrechts-Universität zu Kiel, Germany, after etching the surface with 5% HCl for ca. 40 s. Carbonate samples were then extracted with a hand-held dental drill in the case of thick shells or with a computer-controlled micromill at the GeoZentrum Nordbayern. In total, 83 belemnite rostra, seven oyster shells, and three sediment samples were analysed for their stable isotope ($\delta^{13}C$, $\delta^{18}O$) and element (Mg/Ca, Sr/Ca) composition. In addition, iron and manganese contents were measured to check for signs of alteration of the chemical composition.

Stable isotope analyses were conducted using a carbonate preparation device (Kiel IV) connected with a ThermoScientific MAT 253 mass spectrometer at the Leibniz Laboratory for radiometric dating and stable isotope research at the Christian-Albrechts-Universität zu Kiel, Germany. The samples were reacted within the preparation device with 100% orthophosphoric acid at 75 °C and the evolved CO_2 gas was analysed eight times using the mass spectrometer. On daily routine, different laboratory internal carbonate standards and two international carbonate standards were analysed to control the precision of the measured $\delta^{13}C$ and $\delta^{18}O$ values. These include the international carbonate standards NBS-19 ($\delta^{13}C$: + 1.95‰ VPDB; $\delta^{18}O$: –2.20‰ VPDB) and IAEA-603 ($\delta^{13}C$: + 2.46‰ VPDB; $\delta^{18}O$: –2.37‰ VPDB) as well as the laboratory internal carbonate standards Hela1 ($\delta^{13}C$: + 0.91‰ VPDB; $\delta^{18}O$: + 2.48‰ VPDB), HB1 ($\delta^{13}C$: –12.10‰ VPDB; $\delta^{18}O$: –18.10‰ VPDB), and SHK ($\delta^{13}C$: + 1.74‰ VPDB; $\delta^{18}O$: –4.85‰ VPDB). On the basis of the performance of the carbonate standards, the precision was better than ±0.08‰ (1SD) for $\delta^{18}O$ values and better than ±0.05‰ (1SD) for $\delta^{13}C$ values. All measured values are reported in per mil relative to the Vienna Pee Dee Belemnite (VPDB) scale using NBS-19.

Subsequently, samples were dissolved in diluted nitric acid and analysed for their elemental composition by inductively coupled plasma optical emission spectrometry using a Spectro Ciros SOP instrument at the Institut für Geowissenschaften, Christian-Albrechts-Universität zu Kiel, Germany. Average measurement uncertainty for Mg/Ca was around 1.3‰ and for Sr/Ca around 1.2‰ (1SD). Reference materials Coral JCp-1, Tridacna JCt-1 and limestones ECRM-752, Cal-S were used as secondary standards, and measurement results and reference values are compiled in Table 1.

Statistical correlations between datasets were examined using the Spearman correlation coefficient (rs) and linear trend lines were plotted based on reduced major axis (RMA) regression. Potential temporal trends were illustrated using LOESS smoothing with a smoothing factor of 0.5.

5 Results

The analytical results of all samples are listed in Table 2.

5.1 Fossil preservation

Attempts to reconstruct original environmental conditions by using geochemical analyses of fossils require well-preserved material. This can pose problems in many geological settings, and can be expected to be particularly difficult in the Himalayas, where the fossils experienced an intense orogeny with tectonic uplifts of more than 4000 m as well as strong folding and faulting at potentially high temperatures and pressures. Indeed, a large number of fossils in the present collection show macroscopic signs of fracturing, deformation, and recrystallization (Fig. 4). Especially, the material of the Zanskar region was poorly preserved. This apparently poor preservation was also visible in cathodoluminescence microscopy and scanning electron microscopy (Fig. 5). Specimens from the outcrops in the Zanskar Valley were therefore excluded from temperature reconstructions and only eight belemnite rostra were analysed for comparison. In contrast, the state of preservation was more variable in the Spiti Valley and in some cases improved considerably when moving a few meters away from fault zones. Nevertheless, luminescent belemnite rostra were encountered regularly and had to be eliminated from the study. Unfortunately, all oyster shells collected during the field surveys were found to be strongly recrystallized and only seven shells were analysed for comparison.

Since well-preserved belemnites generally show very low iron and manganese contents (e.g. Brand and Veizer 1980, 1981; Marshall 1992; Price and Sellwood 1997; Wierzbowski and Joachimski 2007), cut-off grades can be determined to exclude potentially altered specimens from further interpretations. Consequently, all belemnites with an iron content above 250 μg/g and a manganese content above 50 μg/g were excluded from further interpretation (for similar cut-off grades see Wierzbowski et al. 2009; Nunn

Table 1 Composition of reference materials and measurement results/uncertainties

	Sr/Ca				Mg/Ca				Reference
	Recomm. (mmol/mol)	*U* (mmol/mol)	Measured (mmol/mol)	*u* (mmol/mol)	Recomm. (mmol/mol)	*U* (mmol/mol)	Measured (mmol/mol)	*u* (mmol/mol)	
JCp-1	**8.838**	0.089	**8.851**	0.0155	**4.199**	0.132	**4.229**	0.024	Hathorne et al. 2013
JCt-1	**1.680**	0.055	**1.814**	0.1300	**1.289**	0.092	**1.252**	0.107	Hathorne et al. 2013
ECRM-752			**0.221**	0.0004	**3.824**	0.095	**3.778**	0.008	Greaves et al. 2008
Cal-S	**0.297**	*Info value*	**0.307**	0.0002	**9.7**	*Info value*	**8.918**	0.019	Jochum et al. 2007; Info values

Recomm. Recommended value (robust median); *Measured* Measured value; *U* Expanded uncertainty; *u* Measurement uncertainty

Table 2 Overview on the studied samples from the Spiti and Zanskar valleys in the Indian Himalayas and results of geochemical analyses. The entries in bold indicate iron or manganese contents exceeding the defined cut-off values.

Sample	Taxonomy	Section	Coordinates	Lithostratigraphy	Age	Relative stratigraphy[a]	$\delta^{13}C$ (‰ VPDB)	$\delta^{18}O$ (‰ VPDB)	T (°C)[b]	T (°C)[c]	Mg/Ca (mmol/mol)	T (°C)[d]	Sr/Ca (mmol/mol)	Fe (μg/g)	Mn (μg/g)
Spiti Valley															
Accepted specimens															
SP16-001	Belemnite	Langza	N 32.2675, E 78.0786	Lower member	M. Callovian–Oxfordian	2.95	−0.19	−2.81	23.9	35.3	10.64	19.8	1.561	213	<30
SP16-003	Belemnite	Langza	N 32.2675, E 78.0786	Lower member	M. Callovian–Oxfordian	2.95	−0.19	−4.07	29.9	42.3	9.743	19.0	1.235	174	<30
SP16-004	Belemnite	Langza	N 32.2675, E 78.0786	Lower member	M. Callovian–Oxfordian	2.95	−0.03	−2.73	23.6	34.9	13.04	21.7	1.476	163	<30
SP16-005	Belemnite	Langza	N 32.2675, E 78.0786	Lower member	M. Callovian–Oxfordian	3.98	0.04	−2.54	22.7	33.8	11.34	20.4	1.391	<90	<30
SP16-006	Belemnite	Langza	N 32.2675, E 78.0786	Lower member	M. Callovian–Oxfordian	3.98	0.49	−0.59	14.3	23.7	11.38	20.4	1.742	<90	<30
SP16-007	Belemnite	Langza	N 32.2675, E 78.0786	Lower member	M. Callovian–Oxfordian	3.98	−0.20	−3.05	25.0	36.6	11.95	20.9	1.405	145	<30
SP16-074	Belemnite	Kibber	N 32.3244, E 78.0069	Lower member	M. Callovian–Oxfordian	4.13	0.96	−3.68	28.0	40.1	10.60	19.8	1.370	214	40
SP16-075	Belemnite	Kibber	N 32.3244, E 78.0069	Lower member	M. Callovian–Oxfordian	4.13	1.06	−2.32	21.7	32.6	4.721	12.5	1.764	<90	<30
SP16-076	Belemnite	Kibber	N 32.3244, E 78.0069	Lower member	M. Callovian–Oxfordian	4.13	−0.15	−1.91	19.9	30.5	7.193	16.3	1.310	145	<30
SP18-011	Belemnite	Hikkim	N 32.2388, E 78.0788	Lower member	M. Callovian–Oxfordian	4.13	0.00	−3.24	25.9	37.7	13.19	21.8	1.293	217	<30
SP18-012	Belemnite	Hikkim	N 32.2388, E 78.0788	Lower member	M. Callovian–Oxfordian	4.13	−0.75	−4.74	33.3	46.1	16.39	23.8	1.084	<90	<30
SP18-014	Belemnite	Hikkim	N 32.2388, E 78.0788	Lower member	M. Callovian–Oxfordian	4.13	−0.07	−1.52	18.2	28.4	11.60	20.6	1.672	<90	<30
SP16-008	Belemnite	Langza	N 32.2675, E 78.0786	Lower member	M. Callovian–Oxfordian	4.34	−1.23	−2.61	23.0	34.2	9.797	19.1	1.342	125	<30
SP16-009	Belemnite	Langza	N 32.2675, E 78.0786	Lower member	M. Callovian–Oxfordian	4.80	−0.71	−2.47	22.3	33.4	13.89	22.3	1.309	228	<30
SP16-011	Belemnite	Langza	N 32.2675, E 78.0786	Lower member	M. Callovian–Oxfordian	11.46	1.38	−0.87	15.5	25.1	8.474	17.8	1.380	<90	<30
SP16-012	Belemnite	Langza	N 32.2675, E 78.0786	Lower member	M. Callovian–Oxfordian	11.46	1.22	−1.55	18.3	28.6	11.08	20.2	1.640	219	<30
SP16-017a	Belemnite	Langza	N 32.2675, E 78.0786	Lower member	M. Callovian–Oxfordian	19.60	−0.26	−2.85	24.1	35.5	12.18	21.1	1.216	186	<30
SP16-019	Belemnite	Langza	N 32.2675, E 78.0786	Lower member	M. Callovian–Oxfordian	24.20	−0.14	−1.17	16.7	26.6	9.283	18.6	1.413	<90	<30
SP18-001	Belemnite	Hikkim	N 32.2429, E 78.0854	Lower member	M. Callovian–Oxfordian	30.52	0.01	−1.36	17.5	27.6	9.437	18.7	1.345	<90	<30
SP18-002	Belemnite	Hikkim	N 32.2429, E 78.0854	Lower member	M. Callovian–Oxfordian	30.52	0.17	−2.43	22.2	33.2	13.25	21.8	1.356	<90	<30
SP18-003	Belemnite	Hikkim	N 32.2429, E 78.0854	Lower member	M. Callovian–Oxfordian	30.52	−0.11	−1.05	16.2	26.0	9.545	18.9	1.268	<90	<30
SP18-004	Belemnite	Hikkim	N 32.2429, E 78.0854	Lower member	M. Callovian–Oxfordian	30.52	0.21	−3.78	28.5	40.7	13.57	22.1	1.268	114	<30
SP18-005	Belemnite	Hikkim	N 32.2429, E 78.0854	Lower member	M. Callovian–Oxfordian	30.52	−0.34	−1.71	19.0	29.4	9.392	18.7	1.197	<90	<30
SP16-021	Belemnite	Langza	N 32.2675, E 78.0786	Middlmember	Kimmeridgian	34.77	0.48	−2.10	20.7	31.5	9.200	18.5	1.425	188	<30
SP16-026	Belemnite	Langza	N 32.2675, E 78.0786	Middlmember	Kimmeridgian	45.28	1.69	−1.95	20.0	30.7	6.884	15.9	1.191	174	<30
SP16-027	Belemnite	Langza	N 32.2675, E 78.0786	Middlmember	Kimmeridgian	45.28	1.67	−2.24	21.3	32.2	9.515	18.8	1.271	233	<30
SP16-031	Belemnite	Langza	N 32.2675, E 78.0786	Middlmember	Kimmeridgian	49.85	1.08	−1.06	16.2	26.0	4.365	11.7	1.417	108	<30
SP16-032	Belemnite	Langza	N 32.2675, E 78.0786	Middlmember	Kimmeridgian	49.85	0.57	−0.43	13.7	22.9	3.909	10.7	1.366	113	<30
SP16-033	Belemnite	Langza	N 32.2675, E 78.0786	Middlmember	Kimmeridgian	49.85	1.22	−0.22	12.8	21.8	3.822	10.5	1.445	<90	<30
SP16-034	Belemnite	Langza	N 32.2675, E 78.0786	Middlmember	Kimmeridgian	49.85	0.78	−0.48	13.9	23.2	4.628	12.3	1.453	<90	<30
SP16-036	Belemnite	Langza	N 32.2675, E 78.0786	Middlmember	Kimmeridgian	49.95	1.39	−0.13	12.5	21.4	3.445	9.6	1.421	<90	<30
SP16-037	Belemnite	Langza	N 32.2675, E 78.0786	Middlmember	Kimmeridgian	49.95	−0.33	0.14	11.4	20.1	5.617	14.0	1.437	<90	<30
SP16-038	Belemnite	Langza	N 32.2675, E 78.0786	Middlmember	Kimmeridgian	49.95	1.05	0.03	11.9	20.6	5.433	13.7	1.608	<90	<30
SP16-040	Belemnite	Langza	N 32.2675, E 78.0786	Middlmember	Kimmeridgian	50.15	0.34	−0.36	13.4	22.6	4.984	12.9	1.448	<90	<30

Table 2 Overview on the studied samples from the Spiti and Zanskar valleys in the Indian Himalayas and results of geochemical analyses. The entries in bold indicate iron or manganese contents exceeding the defined cut-off values. *(Continued)*

Sample	Taxonomy	Section	Coordinates	Lithostratigraphy	Age	Relative stratigraphy[a]	$\delta^{13}C$ (‰ VPDB)	$\delta^{18}O$ (‰ VPDB)	T (°C)[b]	T (°C)[c]	Mg/Ca (mmol/mol)	T (°C)[d]	Sr/Ca (mmol/mol)	Fe (μg/g)	Mn (μg/g)
SP16-043	Belemnite	Langza	N 32.2675, E 78.0786	Middlmember	Kimmeridgian	50.25	0.51	−0.26	13.0	22.1	3.865	10.6	1.350	<90	<30
SP16-044	Belemnite	Langza	N 32.2675, E 78.0786	Middlmember	Kimmeridgian	50.35	0.50	0.03	11.9	20.6	5.060	13.1	1.454	142	<30
SP16-045	Belemnite	Langza	N 32.2675, E 78.0786	Middlmember	Kimmeridgian	50.45	1.26	−0.48	13.9	23.1	5.961	14.6	1.725	<90	<30
SP16-046	Belemnite	Langza	N 32.2675, E 78.0786	Middlmember	Kimmeridgian	50.45	0.85	0.20	11.2	19.8	5.018	13.0	1.388	<90	<30
SP16-047	Belemnite	Langza	N 32.2675, E 78.0786	Middlmember	Kimmeridgian	50.45	1.01	−0.32	13.2	22.3	4.944	12.9	1.514	<90	<30
SP16-048	Belemnite	Langza	N 32.2675, E 78.0786	Middlmember	Kimmeridgian	50.55	1.42	0.35	10.6	19.0	4.673	12.4	1.462	<90	<30
SP16-049	Belemnite	Langza	N 32.2675, E 78.0786	Middlmember	Kimmeridgian	50.55	0.61	−0.71	14.8	24.3	4.213	11.4	1.267	125	<30
SP16-050	Belemnite	Langza	N 32.2675, E 78.0786	Middlmember	Kimmeridgian	50.65	1.46	0.45	10.3	18.6	3.687	10.2	1.395	<90	<30
SP16-051	Belemnite	Langza	N 32.2675, E 78.0786	Middlmember	Kimmeridgian	50.65	−0.10	0.41	10.4	18.8	3.419	9.5	1.293	<90	<30
SP16-052	Belemnite	Langza	N 32.2675, E 78.0786	Middlmember	Kimmeridgian	50.75	0.40	−0.32	13.2	22.3	6.540	15.4	1.592	107	<30
SP16-053a	Belemnite	Langza	N 32.2675, E 78.0786	Middlmember	Kimmeridgian	50.75	1.03	−0.63	14.5	23.9	7.484	16.6	1.563	128	<30
SP16-056	Belemnite	Langza	N 32.2675, E 78.0786	Middlmember	Kimmeridgian	50.99	0.56	0.63	9.6	17.7	6.118	14.8	1.404	<90	<30
SP16-057	Belemnite	Langza	N 32.2675, E 78.0786	Middlmember	Kimmeridgian	51.42	0.84	−2.37	21.9	32.9	8.154	17.4	1.373	250	<30
SP16-066a	Belemnite	Demul	N 32.1519, E 78.1719	?Upper member	Early Tithonian	56.70	0.08	0.37	10.6	19.0	4.874	12.7	1.484	<90	<30
SP16-064	Belemnite	Gete	N 32.3053, E 78.0219	Upper member	LatTithonian	58.70	−1.43	−3.75	28.4	40.5	4.814	12.6	1.547	96	<30
SP16-067	Belemnite	Demul	N 32.1500, E 78.1750	Upper member	LatTithonian	58.92	0.07	−0.50	14.0	23.2	7.652	16.8	1.705	150	<30
SP16-068	Belemnite	Demul	N 32.1500, E 78.1750	Upper member	LatTithonian	58.92	1.15	0.03	11.9	20.6	6.475	15.3	1.363	<90	<30
SP16-069	Belemnite	Demul	N 32.1500, E 78.1750	Upper member	LatTithonian	58.92	0.16	0.65	9.5	17.6	4.498	12.0	1.533	<90	<30
SP16-070	Belemnite	Demul	N 32.1500, E 78.1750	Upper member	LatTithonian	58.92	0.94	0.57	9.8	18.0	4.829	12.7	1.434	98	<30
SP18-018	Belemnite	Demul	N 32.1500, E 78.1750	Upper member	LatTithonian	58.92	0.48	−0.08	12.3	21.1	5.174	13.3	1.519	<90	<30
SP18-019	Belemnite	Demul	N 32.1500, E 78.1750	Upper member	LatTithonian	59.70	1.02	−1.10	16.4	26.3	5.655	14.1	1.325	147	<30
SP18-020	Belemnite	Demul	N 32.1500, E 78.1750	Upper member	LatTithonian	59.70	1.50	0.24	11.1	19.6	4.948	12.9	1.177	<90	<30
SP18-021	Belemnite	Demul	N 32.1500, E 78.1750	Upper member	LatTithonian	59.70	1.82	−0.55	14.2	23.5	6.667	15.6	1.636	<90	<30
SP18-006	Belemnite	Demul	N 32.1500, E 78.1750	Upper member	LatTithonian	62.70	1.39	−0.29	13.1	22.2	4.550	12.1	1.264	109	<30
SP18-007	Belemnite	Demul	N 32.1500, E 78.1750	Upper member	LatTithonian	62.70	0.43	0.22	11.1	19.7	5.324	13.5	1.151	143	<30
SP18-009	Belemnite	Demul	N 32.1500, E 78.1750	Upper member	LatTithonian	62.70	1.42	−0.20	12.8	21.7	7.703	16.9	1.365	<90	<30
SP18-010	Belemnite	Demul	N 32.1500, E 78.1750	Upper member	LatTithonian	62.70	0.89	−1.37	17.5	27.6	9.044	18.4	1.588	<90	<30
Discarded specimens															
SP16-060	Oyster	Chichim	N 32.3469, E 77.9688	Tagling Formation	?Bathonian	-	1.52	−8.20	(52.5)	-	4.968	-	0.678	**653**	<30
SP16-061A+B	Oyster	Chichim	N 32.3469, E 77.9688	Tagling Formation	?Bathonian	-	1.61	−8.85	(56.5)	-	8.506	-	0.748	**1014**	<30
SP16-062	Oyster	Chichim	N 32.3469, E 77.9688	Tagling Formation	?Bathonian	-	1.24	−8.70	(55.6)	-	3.713	-	0.743	**381**	<30
SP16-014	Belemnite	Langza	N 32.2675, E 78.0786	Lower member	M. Callovian–Oxfordian	?	0.62	−2.90	(24.3)	(35.8)	10.01	(19.3)	1.316	**1028**	<30
SP16-015	Belemnite	Langza	N 32.2675, E 78.0786	Lower member	M. Callovian–Oxfordian	?	0.69	−4.93	(34.3)	(47.3)	10.53	(19.7)	1.319	**1062**	34
SP16-002	Belemnite	Langza	N 32.2675, E 78.0786	Lower member	M. Callovian–Oxfordian	2.95	−0.02	−8.77	(56.0)	(71.6)	13.58	(22.1)	1.116	**379**	<30
SP18-015	Belemnite	Hikkim	N 32.2388, E 78.0788	Lower member	M. Callovian–Oxfordian	4.13	−0.91	−3.89	(29.0)	(41.2)	17.99	(24.6)	1.278	**1329**	<30
SP16-013	Belemnite	Langza	N 32.2675, E 78.0786	Lower member	M. Callovian–Oxfordian	11.46	−1.30	−11.66	(74.9)	(92.5)	10.88	(20.0)	0.860	**1114**	<30

Table 2 Overview on the studied samples from the Spiti and Zanskar valleys in the Indian Himalayas and results of geochemical analyses. The entries in bold indicate iron or manganese contents exceeding the defined cut-off values. *(Continued)*

Sample	Taxonomy	Section	Coordinates	Lithostratigraphy	Age	Relative stratigraphy[a]	$\delta^{13}C$ (‰ VPDB)	$\delta^{18}O$ (‰ VPDB)	T (°C)[b]	T (°C)[c]	Mg/Ca (mmol/mol)	T (°C)[d]	Sr/Ca (mmol/mol)	Fe (µg/g)	Mn (µg/g)
SP16-059a	Oyster	Langza	N 32.2675, E 78.0786	Lower member	M. Callovian–Oxfordian	12.82	1.57	−10.58	(67.6)	-	3.231	-	-	**263**	<30
SP16-016	Belemnite	Langza	N 32.2675, E 78.0786	Lower member	M. Callovian–Oxfordian	19.60	1.47	−3.02	(24.9)	(36.4)	8.527	(17.8)	1.458	**303**	<30
SP16-022	Belemnite	Langza	N 32.2675, E 78.0786	Middlmember	Kimmeridgian	34.77	−0.19	−4.12	(30.2)	(42.6)	12.32	(21.2)	1.239	**373**	<30
SP16-023	Oyster	Langza	N 32.2675, E 78.0786	Middlmember	Kimmeridgian	34.77	2.76	−10.76	(68.8)	-	2.869	-	0.537	**10299**	**442**
SP16-024	Oyster	Langza	N 32.2675, E 78.0786	Middlmember	Kimmeridgian	34.77	−0.04	−9.71	(61.9)	-	6.989	-	0.637	**3458**	**75**
SP16-025	Oyster	Langza	N 32.2675, E 78.0786	Middlmember	Kimmeridgian	34.77	3.33	−10.76	(68.8)	-	1.343	-	0.581	**1267**	<30
SP16-029	Belemnite	Langza	N 32.2675, E 78.0786	Middlmember	Kimmeridgian	47.51	1.04	−2.22	(21.2)	(32.1)	6.050	(14.7)	1.336	**259**	<30
SP16-030	Belemnite	Langza	N 32.2675, E 78.0786	Middlmember	Kimmeridgian	47.51	1.75	−1.12	(16.5)	(26.4)	6.887	(15.9)	1.236	**1781**	**130**
SP16-035	Belemnite	Langza	N 32.2675, E 78.0786	Middlmember	Kimmeridgian	49.95	0.23	−0.73	(14.9)	(24.4)	4.633	(12.3)	1.236	**261**	<30
SP16-042	Belemnite	Langza	N 32.2675, E 78.0786	Middlmember	Kimmeridgian	50.15	1.24	−0.34	(13.3)	(22.5)	4.264	(11.5)	1.380	**608**	<30
SP16-058	Belemnite	Langza	N 32.2675, E 78.0786	Middlmember	Kimmeridgian	51.42	−0.09	−2.69	(23.4)	(34.6)	8.465	(17.8)	1.233	**392**	<30
SP16-071	Belemnite	Demul	N 32.1500, E 78.1750	Upper member	LatTithonian	58.92	0.65	0.35	(10.6)	(19.0)	6.345	(15.1)	1.315	**353**	37
SP16-072	Belemnite	Demul	N 32.1500, E 78.1750	Upper member	LatTithonian	58.92	1.11	0.45	(10.3)	(18.6)	6.717	(15.7)	1.449	**2031**	**85**
Sediment samples															
SP16-059b	Sediment	Langza	N 32.2675, E 78.0786	Lower member	M. Callovian–Oxfordian	12.82	−0.27	−10.90	-	-	25.72	-	0.864	**12493**	**278**
SP16-017b	Sediment	Langza	N 32.2675, E 78.0786	Lower member	M. Callovian–Oxfordian	19.60	−2.97	−10.11	-	-	27.25	-	0.810	**19545**	**235**
SP16-053b	Sediment	Langza	N 32.2675, E 78.0786	Middlmember	Kimmeridgian	50.75	−3.68	−10.71	-	-	14.27	-	0.615	**38443**	**512**
Zanskar Valley															
Discarded specimens															
ZA18-007	Belemnite	Rangdum NE	N 34.0626, E 76.4248	Ferruginous OolitFormation	?Callovian	-	−0.58	−9.93	(63.4)	(79.7)	12.80	(21.5)	1.546	230	<30
ZA18-008	Belemnite	Rangdum NE	N 34.0626, E 76.4248	Ferruginous OolitFormation	?Callovian	-	−0.28	−10.94	(70.0)	(87.0)	9.940	(19.2)	1.293	**877**	<30
ZA18-009	Belemnite	Rangdum NE	N 34.0626, E 76.4248	Ferruginous OolitFormation	?Callovian	-	−0.11	−10.72	(68.5)	(85.4)	10.67	(19.9)	1.340	**561**	<30
ZA18-001	Belemnite	Zangla Village	N 33.6658, E 76.9861	Lower member	M. Callovian–Oxfordian	-	−0.71	−11.55	(74.1)	(91.7)	12.16	(21.1)	1.727	**3844**	**163**
ZA18-002	Belemnite	Zangla Village	N 33.6658, E 76.9861	Lower member	M. Callovian–Oxfordian	-	0.25	−7.55	(48.7)	(63.4)	4.091	(11.1)	1.744	**513**	36
ZA18-003	Belemnite	Zangla Cliff	N 33.6828, E 76.9717	Lower member	M. Callovian–Oxfordian	-	−0.31	−8.36	(53.5)	(68.8)	4.870	(12.7)	1.348	110	<30
ZA18-004	Belemnite	Zangla Cliff	N 33.6828, E 76.9717	Lower member	M. Callovian–Oxfordian	-	1.73	−7.08	(46.0)	(60.4)	4.768	(12.5)	1.336	156	<30
ZA18-010	Belemnite	Zangla Village	N 33.6658, E 76.9875	Lower member	M. Callovian–Oxfordian	-	−0.08	−8.48	(54.2)	(69.6)	6.076	(14.7)	1.430	**901**	**69**

[a]The relative stratigraphy represents the position of the sample in the composite section of Figure 6 in meters
[b]Temperatures are calculated with the equation of Anderson and Arthur (1983) and a $\delta^{18}O_{sea}$ value of −1‰ VSMOW during shell formation (Shackleton and Kennett 1975)
[c]Temperatures are calculated with the equation of Daëron et al. (2019) and a $\delta^{18}O_{sea}$ value of −0.2‰ VSMOW during shell formation
[d]Temperatures are calculated with the equation of Nunn and Price (2010)

Fig. 4 Field photographs of poorly preserved belemnites from the Spiti Shale Formation documenting the effects of the Himalayan orogeny. **a, b** Strongly fractured belemnites in the Upper member near Gete in the Spiti Valley; **c, d** Fractured, recrystallized, and deformed belemnites concentrated in a shell bed near Zangla in the Zanskar Valley

and Price 2010; Alberti et al. 2012b, 2020b; Arabas et al. 2017). Analyses of sediment samples showed high iron and manganese contents pointing to the presence of both elements in the system. However, in the analysed belemnites, manganese contents were mostly negligible and below the detection limit (even for the poorly preserved samples from Zanskar), but elevated iron contents led to the exclusion of a number of samples from interpretation. Of the 83 belemnite rostra analysed, 61 specimens showed acceptable iron and manganese contents. Only data of these specimens were used for interpretations in the following sections (compare Table 2).

Another potential indicator for diagenetic alteration is a positive correlation between $\delta^{13}C$ and $\delta^{18}O$ values in the dataset (Fig. 6a) since burial generally leads to a decrease in both values (Hodgson 1966; Hudson 1977; Nelson and Smith 1996; Ullmann and Korte 2015). This can be seen particularly well in the extremely negative $\delta^{18}O$ values of all bivalve shells and some of the discarded belemnite rostra. At the same time, $\delta^{13}C$ values of the potentially altered specimens are not lower than those of the more well-preserved specimens. Furthermore, some of the belemnite rostra with low iron and manganese contents still show surprisingly negative $\delta^{18}O$ values, but not necessarily very low $\delta^{13}C$ values. It seems therefore likely that even some of the accepted specimens that passed all tests for diagenetic alteration exhibit some (limited?) change in their chemical composition. Such a comparatively light influence of diagenetic alteration on some of the accepted samples might also explain the weak positive correlation between $\delta^{13}C$ and $\delta^{18}O$ values in the dataset ($r_s = 0.43$; $p < 0.05$; Fig. 6a). In this regard, the presented data have to be considered with some caution.

5.2 Results of the geochemical analyses

While Table 2 lists all analytical results, Table 3 lists average stable isotope values and element ratios for the 61 accepted belemnite rostra representing Middle Callovian–Oxfordian, Kimmeridgian, and Tithonian ages. The $\delta^{13}C$ values of the accepted samples fluctuate between −1.43‰ and +1.82‰ (Table 2; Fig. 7a). While the measured $\delta^{13}C$ values vary around an average of +0.05‰ in the Middle Callovian–Oxfordian, they

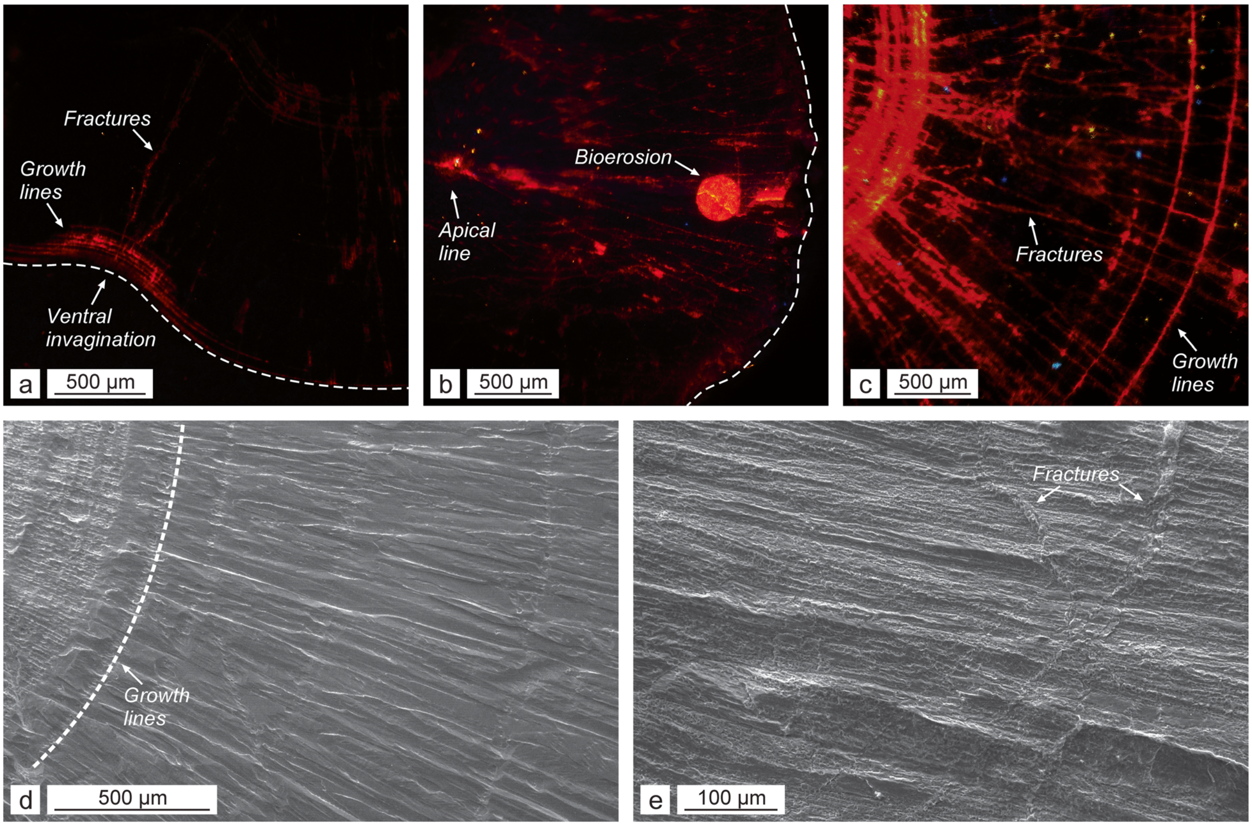

Fig. 5 a – c Cathodoluminescence microscopy revealed the common occurrence of luminescent fractures and growth lines in the collected belemnites, particularly around the apical line and the ventral invagination. Traces of bioerosion are comparatively sparse. While a considerable number of belemnite samples from the Spiti Valley contains dark areas, all rostra from the Zanskar Valley are strongly luminescent reflecting considerable alteration. Only samples from non-luminescent areas, believed to be at least moderately well-preserved, were used for palaeoenvironmental reconstructions (**a:** SP16-066 from the Upper member near Demul, Spiti Valley; **b:** SP18-022 from the Upper member near Demul, Spiti Valley; **c:** ZA18-003 from the Lower member near Zangla Cliff, Zanskar Valley); **d, e** Scanning electron microscopy demonstrates varying levels of preservation among the studied fossils. Well-preserved belemnite rostra show comparatively regular, radial calcite crystals without signs of alteration or fractures (**d:** SP16-069 from the Upper member near Demul, Spiti Valley). In contrast, all studied oysters are poorly preserved with abundant fractures crossing the partly recrystallized shell layers (**e:** SP16-023 from the Middle member near Langza, Spiti Valley)

increase towards the Kimmeridgian and decrease only slightly in the Tithonian (Table 3).

The measured $\delta^{18}O$ values vary between − 4.74‰ and + 0.65‰ (Table 2; Fig. 7b) and show a general increase from the Middle Callovian–Oxfordian through the Kimmeridgian to the Tithonian (Table 3). This long-term trend is overlain by small-scale fluctuations, which seem to indicate a rather weak increase in $\delta^{18}O$ values from the Middle Callovian–Oxfordian until the mid-Kimmeridgian, followed by a stronger increase towards the Kimmeridgian–Tithonian boundary, and a slight decrease in values from the Early to the Late Tithonian. However, these short-term fluctuations might be exaggerated by the limited number of samples for some of the stratigraphic levels.

The Mg/Ca ratios fluctuate between 3.42 and 16.39 mmol/mol (Table 2; Fig. 7c). In general, the values are relatively high throughout the Middle Callovian–Oxfordian, drop significantly within the Kimmeridgian, and increase only slightly again in the Tithonian (Table 3). This way, the Mg/Ca ratios show an inverse trend compared to the $\delta^{18}O$ values and both values are indeed negatively correlated ($rs = -0.73$; $p < 0.05$; Fig. 6b).

The Sr/Ca ratios vary between 1.08 and 1.76 mmol/mol (Table 2; Fig. 7d) and fluctuate only very slightly through time. While average values indicate a weak, but steady increase from the Middle Callovian–Oxfordian to the Tithonian, the magnitude of this change is almost negligible (Table 3). The Sr/Ca ratios show no significant correlation with $\delta^{18}O$ values ($rs = 0.21$; $p = 0.11$; Fig. 6c).

6 Discussion

6.1 The $\delta^{18}O$ value of seawater

The ratio between the stable oxygen isotopes ^{18}O and ^{16}O within a shell (represented by the $\delta^{18}O_{shell}$ value) is mainly a function of the original ratio within the ocean

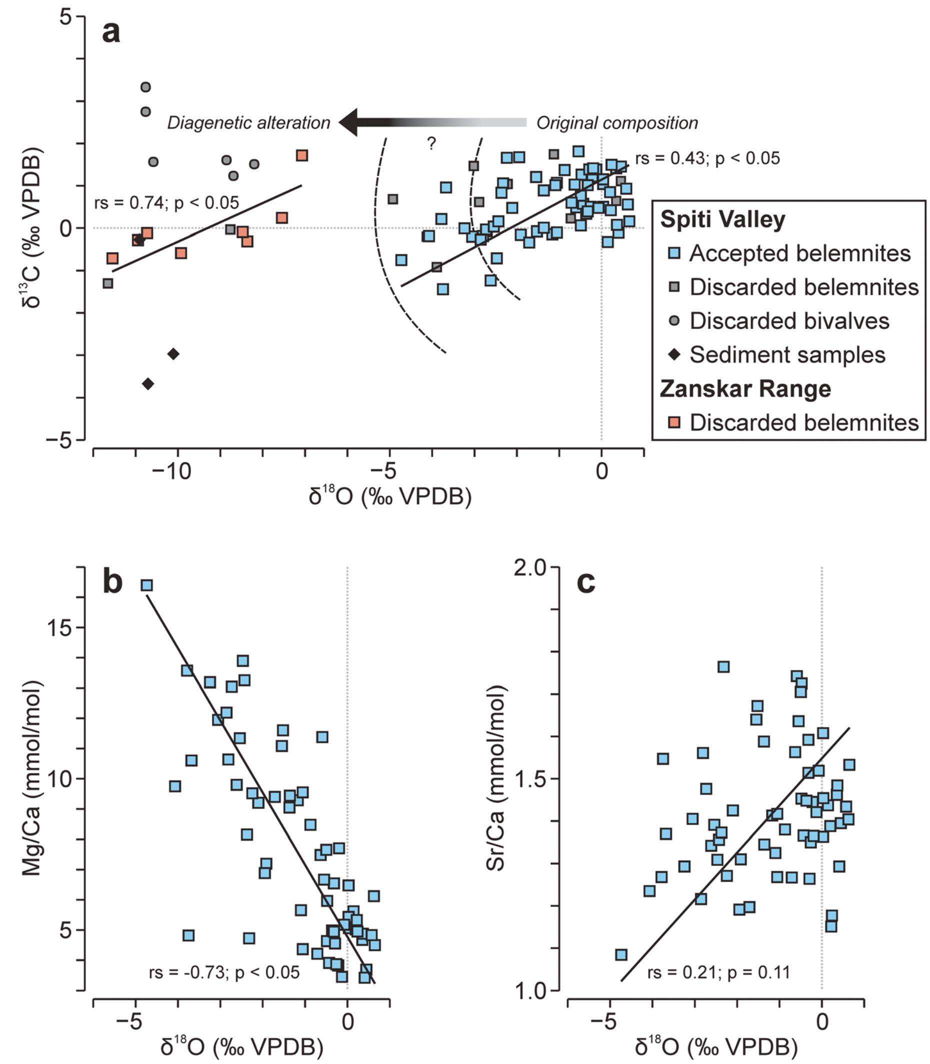

Fig. 6 a A bivariate plot of $\delta^{18}O$ versus $\delta^{13}C$ values of all samples shows that alteration leads to successively more negative $\delta^{18}O$ values in the analysed fossils from the Spiti and Zanskar valleys. Note the significant correlation between the $\delta^{18}O$ and $\delta^{13}C$ values of the belemnites from the Zanskar Valley; **b** A bivariate plot of $\delta^{18}O$ versus Mg/Ca values of the accepted belemnites from the Spiti Valley exhibits a strong negative correlation; **c** A bivariate plot of $\delta^{18}O$ versus Sr/Ca values of the accepted belemnites from the Spiti Valley does not show any correlation

Table 3 Summary of analytical results and temperature estimates based on different methods for the Middle Callovian–Oxfordian, Kimmeridgian, and Tithonian

	Middle Callovian–Oxfordian	Kimmeridgian	Tithonian
Number of specimens	23	24	14
Average $\delta^{13}C$ (‰ VPDB)	0.05	0.85	0.71
Average $\delta^{18}O$ (‰ VPDB)	−2.39	−0.49	−0.41
Average Mg/Ca (mmol/mol)	10.94	5.456	5.872
Average Sr/Ca (mmol/mol)	1.393	1.428	1.435
T (°C); Anderson and Arthur (1983); $\delta^{18}O_{sea} = -1‰$	22.0	13.9	13.6
T (°C); Anderson and Arthur (1983); $\delta^{18}O_{sea} = -0.2‰$	25.7	17.2	16.9
T (°C); Daëron et al. (2019); $\delta^{18}O_{sea} = -1‰$	28.8	19.3	18.9
T (°C); Daëron et al. (2019); $\delta^{18}O_{sea} = -0.2‰$	33.0	23.2	22.8
T (°C); Nunn and Price (2010)	20.1	13.8	14.4

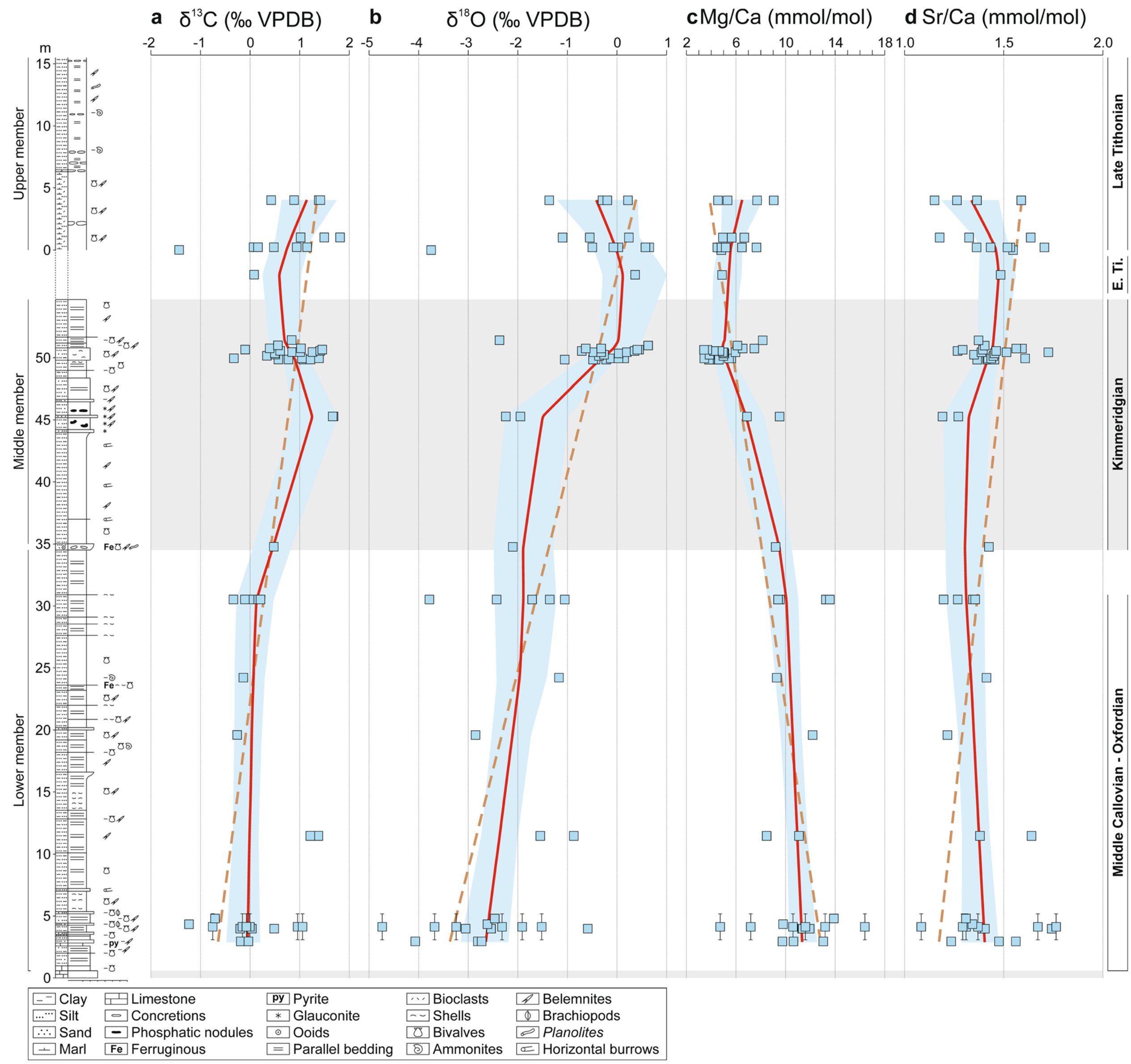

Fig. 7 Results of the $\delta^{13}C$, $\delta^{18}O$, Mg/Ca, and Sr/Ca analyses of the accepted belemnites from the Middle to Upper Jurassic Spiti Shale Formation of the Spiti Valley. The illustrated sections were measured at Langza (Lower and parts of the Middle member) and Demul (parts of the Upper member). Note that these sections do not represent the entire Spiti Shale Formation, but only the sampled part of the succession

water ($\delta^{18}O_{sea}$) and the water temperature during shell precipitation. Reconstructions of water temperatures based on stable oxygen isotope analyses therefore require a reasonable assumption for the $\delta^{18}O_{sea}$ value. The majority of research articles concerned with the Jurassic time interval use a $\delta^{18}O_{sea}$ value of – 1‰ to account for an apparent lack of polar glaciations (compare Shackleton and Kennett 1975). Local to regional influences such as freshwater influx or enhanced evaporation can alter this value (e.g. Alberti et al. 2020b), but it seems unlikely that such factors affected the open-marine setting of the Spiti Shale Formation. Nevertheless, even the $\delta^{18}O_{sea}$ value of open ocean water is not uniform, but changes strongly along a latitudinal gradient with considerably higher $\delta^{18}O_{sea}$ values in low latitudes compared to high latitudes (e.g. $\delta^{18}O_{sea}$ values higher than + 1‰ in the tropics and below – 3‰ in polar waters can be observed in today's oceans; e.g. LeGrande and Schmidt 2006). It is highly likely that such a latitudinal gradient also existed in Earth's history (e.g. Zachos et al. 1994; Roche et al. 2006; Alberti et al. 2020a). It is therefore necessary to consider the palaeogeographical position of study areas for temperature reconstructions. Since the Himalayan strata were strongly compressed laterally during orogeny, it is difficult to reconstruct the exact palaeolatitude for the sample localities, but it seems most likely that the study area was situated somewhere between 20°S to 30°S during the Late Jurassic (Fig. 8; compare data from the so-called Paleolatitude Calculator of van Hinsbergen et al. 2015). These intermediate latitudes show a steep incline in the $\delta^{18}O_{sea}$ gradient with potential absolute values between 0.0 and – 0.4‰ following approximations of Zachos et al. (1994) and Alberti et al. (2020a). Because the Late Jurassic was characterized by the drift of eastern Gondwana into higher latitudes, it additionally seems likely that the palaeolatitude changed by up to 10° during the analysed time interval (Fig. 8). Consequently, the $\delta^{18}O_{sea}$ value for the study area might have been higher in the Middle Callovian–Oxfordian compared to the Tithonian. Recently, clumped isotope analyses have been used in attempts to independently reconstruct water temperatures and $\delta^{18}O_{sea}$ values for selected regions and time intervals in the Mesozoic (e.g. Wierzbowski et al. 2018; Price et al. 2020; Vickers et al. 2020; Fernandez et al. 2021). However, such data are not yet available for Indian study areas and the available approximations for other regions often show very wide ranges from below – 2‰ to above + 2‰ depending on the exact locality, palaeolatitude, time interval, and methodology (compare Wierzbowski et al. 2018; Price et al. 2020; Vickers et al. 2020; Fernandez et al. 2021). While some of these values are comparable to previously proposed $\delta^{18}O_{sea}$ values, others would lead to the calculation of unrealistically warm or cold water temperatures. While some studies were successful to capture large-scale trends (e.g. Wierzbowski et al. 2018; Price et al. 2020), it seems that more research has to be done until clumped isotope analyses can be used systematically to improve temperature reconstructions at high temporal and regional resolutions (compare also Bajnai et al. 2018; Davies et al. 2021). Due to these reasons, temperatures in the present study were reconstructed for a traditionally and commonly used $\delta^{18}O_{sea}$ value of – 1‰ and additionally for a $\delta^{18}O_{sea}$ value of – 0.2‰ representing a subtropical latitude with comparatively high evaporation (following the method of Alberti et al. 2020a).

6.2 Different temperature equations

Since the first researchers started to use stable oxygen isotope analyses for palaeoenvironmental reconstructions, several equations were proposed to translate

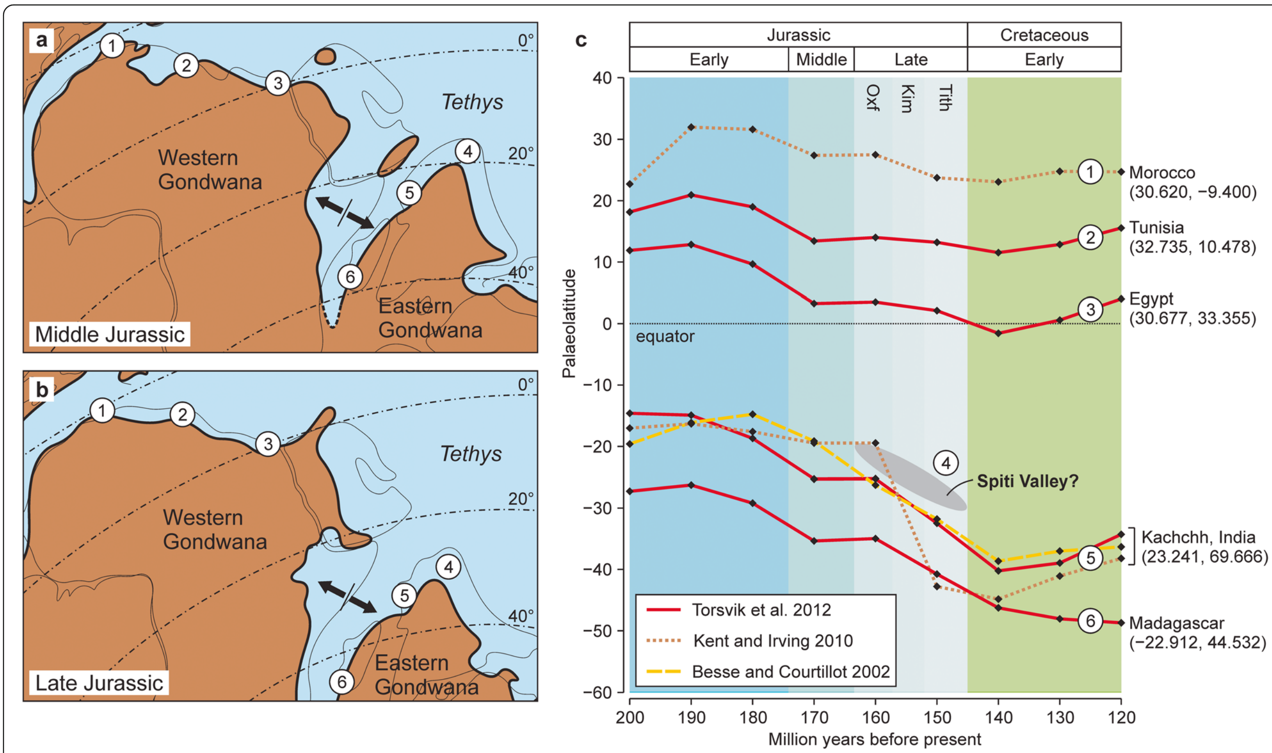

Fig. 8 a, b Palaeogeographic maps for parts of Gondwana for the Middle and Late Jurassic (modified after Enay and Cariou 1997; Alberti et al. 2015). Note that the position of western Gondwana did not change considerably, while eastern Gondwana drifted into higher latitudes; **c** Changes in palaeolatitude through time for selected study areas in western and eastern Gondwana from the Jurassic to the Early Cretaceous (data from the Paleolatitude Calculator; Besse and Courtillot 2002; Kent and Irving 2010; Torsvik et al. 2012; van Hinsbergen et al. 2015). The position of the Spiti Valley is approximated since the extent of lateral compression during the Himalayan orogeny is unknown

$\delta^{18}O_{shell}$ values of calcitic fossils into water temperatures (e.g. Epstein et al. 1951, 1953; Craig 1965; O'Neil et al. 1969). Research on the exact relationship of $\delta^{18}O_{shell}$ values and temperatures is still on-going and more equations are used and developed until today (e.g. Anderson and Arthur 1983; Kim and O'Neil 1997; Leng and Marshall 2004; Takayanagi et al. 2013). Considering their application in temperature reconstructions in deep time (which by nature has to deal with a number of uncertainties), most of these equations result in comparable temperatures with only minor differences. Hence, the majority of studies on Jurassic temperature reconstructions uses the equation of Anderson and Arthur (1983), thereby also enabling an easier comparison of datasets:

$$T(^{\circ}C) = 16 - 4.14 \cdot (\delta^{18}O_{shell} - \delta^{18}O_{sea}) + 0.13 \cdot (\delta^{18}O_{shell} - \delta^{18}O_{sea})^2 \quad (1)$$

However, all of the aforementioned equations cannot explain the striking phenomenon that belemnite rostra generally show higher $\delta^{18}O_{shell}$ values than, for example, co-occurring calcitic bivalve and brachiopod shells (e.g. Prokoph et al. 2008; Mutterlose et al. 2010; Dera et al. 2011; Alberti et al. 2012a, 2019). This almost systematic difference translates into reconstructed temperatures for belemnites, which are commonly around 5 °C lower than those of other taxa. A number of processes have been suggested to explain this discrepancy including differences in life habits (e.g. a migratory behaviour of belemnites) or shell precipitation (e.g. Mutterlose et al. 2010; Hoffmann and Stevens 2019). Most recently, comparisons between the chemical composition of exceptionally preserved belemnite rostra and phragmocones as well as new clumped isotope data support the theory that previously suggested temperature equations are not applicable for $\delta^{18}O_{shell}$ values of belemnites and in fact lead to a consistent underestimation of temperatures (Price et al. 2015; Vickers et al. 2020). In contrast, these authors suggest that $\delta^{18}O_{shell}$ values of belemnites should be translated into water temperatures by using equations of low-precipitation rate experiments (e.g. Coplen 2007; Kele et al. 2015; Daëron et al. 2019). Since research in this area is still debated (compare Bajnai et al. 2018; Davies et al. 2021) and in order to show the magnitude of differences between both methods, the current study presents results based on Anderson and Arthur (1983) as well as the equation of Daëron et al. (2019):

$$1000 \cdot \ln \alpha = 17.57 \cdot 1000/T\ (K) - 29.13 \quad (2)$$

In addition to stable oxygen isotopes, a number of element ratios were proposed as temperature proxies. In particular, Mg/Ca ratios are considered to allow temperature reconstructions in a number of taxonomic groups (e.g. Eggins et al. 2003; Cléroux et al. 2008). Based on earlier research on benthic foraminifera by Lear et al. (2002), Nunn and Price (2010) proposed the following temperature equation for Mg/Ca ratios of belemnites:

$$T\ (^{\circ}C) = \ln\ (Mg/Ca/1.2)/0.11 \quad (3)$$

This equation has been used in the meantime by a number of researchers studying Mg/Ca ratios in belemnite rostra (e.g. Price et al. 2018; Alberti et al. 2020b), but the validity of this proxy is still debated. While some authors have found a negative correlation between $\delta^{18}O_{shell}$ values and Mg/Ca ratios in belemnites and proposed temperature as the common cause (e.g. Bailey et al. 2003; McArthur et al. 2007), others have failed to document a correlation and disputed the use of Mg/Ca ratios as a temperature proxy (Li et al. 2013). In the current dataset, there is a significant negative correlation between $\delta^{18}O_{shell}$ values and Mg/Ca ratios for the 61 accepted belemnite rostra ($rs = -0.73$; $p < 0.05$; Fig. 6b), which seems to support a temperature influence. However, the calculation of absolute temperatures based on Mg/Ca ratios faces another problem. Experimental research on a number of molluscan taxa showed that water temperatures indeed determine the Mg/Ca ratios in their shell, but the exact relationship differed drastically between species (e.g. Surge and Lohmann 2008; Mouchi et al. 2013; Bougeois et al. 2016; Tynan et al. 2017). This implies that temperature equations developed for a certain species cannot be easily used for another. The applicability of the equation of Nunn and Price (2010) is therefore uncertain.

Since there is no significant correlation between $\delta^{18}O_{shell}$ values and Sr/Ca ratios (Fig. 6c), it is believed that this element ratio does not indicate temperature conditions in the analysed belemnites, but is instead influenced by the general ocean water chemistry (compare Steuber and Veizer 2002; Ullmann et al. 2013). Sr/Ca ratios of Jurassic seawater were previously reconstructed using a Sr distribution coefficient of 0.32 for belemnites, but this value is difficult to test for these extinct organisms (Ullmann et al. 2013, 2016). In any case, it is noteworthy that the measured absolute values of the Himalayan belemnites largely agree with those of Ullmann et al. (2016) and also show a similar long-term trend with a slight increase from the Middle Callovian –Oxfordian towards the Tithonian in average values and then a slight decrease again in the Late Tithonian. Similarly, there is only a weak correlation between $\delta^{13}C$ and $\delta^{18}O_{shell}$ values in the dataset believed to be caused by few specimens exhibiting a limited degree of alteration (Fig. 6a). In contrast to the largely temperaturedependent $\delta^{18}O_{shell}$ values, $\delta^{13}C$ values can reflect a number of environmental factors and processes from regional changes in primary productivity or upwelling to global events such as the release of isotopically light methane into the atmosphere (e.g. Wierzbowski 2015; Ait-Itto et al. 2017). In the current study, the low number of specimens and low biostratigraphic resolution prevent further interpretations of the $\delta^{13}C$ data or the identification of carbon isotope excursions, but it can be noted that absolute values are comparable to results from adjacent western India and Madagascar (Fürsich et al. 2005; Alberti et al. 2012a, 2012b, 2019).

6.3 Reconstructing regional water temperatures

The discussions in sections 6.1 and 6.2 show that the choice of the adequate $\delta^{18}O_{sea}$ value and temperature equation is crucial for calculating realistic water-temperature estimates. Figure 9 summarizes the relationship between temperature, equation, and choice of $\delta^{18}O_{sea}$ value, thereby illustrating that absolute temperatures can differ by more than 10 °C between the different methods. For example, a $\delta^{18}O_{shell}$ value of − 1‰ corresponds to a water temperature of 16.0 °C when using the equation of Anderson and Arthur (1983) and a $\delta^{18}O_{sea}$ value of − 1‰. The reconstructed temperature increases to 19.4 °C for a $\delta^{18}O_{sea}$ value of − 0.2‰. If we follow recent research suggesting the use of the equation of Daëron et al. (2019) for belemnite rostra, a $\delta^{18}O_{shell}$ value of − 1‰ results in a reconstructed temperature of 21.8 °C for a $\delta^{18}O_{sea}$ value of − 1‰ and of 25.8 °C for a $\delta^{18}O_{sea}$ value of − 0.2‰.

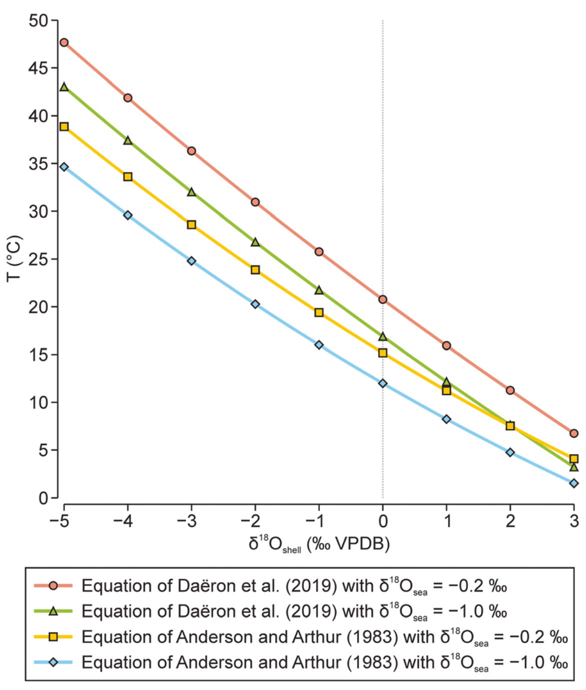

Fig. 9 Comparison of temperature estimates for different $\delta^{18}O_{shell}$ and $\delta^{18}O_{sea}$ values using different equations (Anderson and Arthur 1983; Daëron et al. 2019)

Similar differences in absolute temperature estimates can be found for the Jurassic dataset from the Indian Himalayas (Fig. 10a–d). Table 3 lists the average temperatures for the Middle Callovian–Oxfordian to Tithonian based on both equations and different $\delta^{18}O_{sea}$ values. Since these equations translate the measured $\delta^{18}O_{shell}$ values, the trends through time are the same, only absolute values change. Based on the average values, a continuous temperature decrease can be observed throughout the studied Middle to Late Jurassic time interval. Smoothened trend lines suggest a comparatively weak decrease in the Middle Callovian–Oxfordian and Early Kimmeridgian. Temperatures then drop more prominently towards the Kimmeridgian–Tithonian boundary and remain relatively low in the Early Tithonian, followed by a slight temperature increase into the Late Tithonian. However, the reconstruction of temperature fluctuations at higher temporal resolution might be unreliable due to the scarcity of samples for some horizons and potential diagenetic alteration influencing some specimens.

By following recent research and considering the palaeolatitude of the study area, it seems advisable to use the equation of Daëron et al. (2019) and a $\delta^{18}O_{sea}$ value of − 0.2‰ for the reconstruction of absolute water temperatures (Fig. 10d). While this leads to largely realistic temperature estimates for the Kimmeridgian (average: 23.2 °C) and the Tithonian (average: 22.8 °C), the values for the Middle Callovian–Oxfordian are surprisingly high with an average of 33.0 °C. Several Middle Callovian–Oxfordian belemnites lead to temperature estimates above 35 °C with a maximum of 46.1 °C (SP18-012). While this is a particular problem for this time interval, there is also a prominent outlier in the Late Tithonian with a rather unlikely temperature of 40.5 °C (SP16-064). Such high values suggest diagenetic alteration of some of the specimens and obviously influence the calculation of average temperatures (compare Fig. 6a). Another approach could be to concentrate on the lowest reconstructed temperatures for each time interval: 23.7 °C in the Middle Callovian–Oxfordian (SP16-006), 17.7 °C in the Kimmeridgian (SP16-056), and 17.6 °C in the Tithonian (SP16-069). Even though these minimum temperatures cannot be considered to represent average temperatures of the three time intervals, it is striking that they also reflect a general temperature decrease through time.

Finally, it is likely that the drift of eastern Gondwana into higher latitudes had an effect on the $\delta^{18}O_{sea}$ values. A change in the palaeolatitude from 20°S to 30°S throughout the studied time interval would result in a decrease of the ambient $\delta^{18}O_{sea}$ value by around 0.2‰

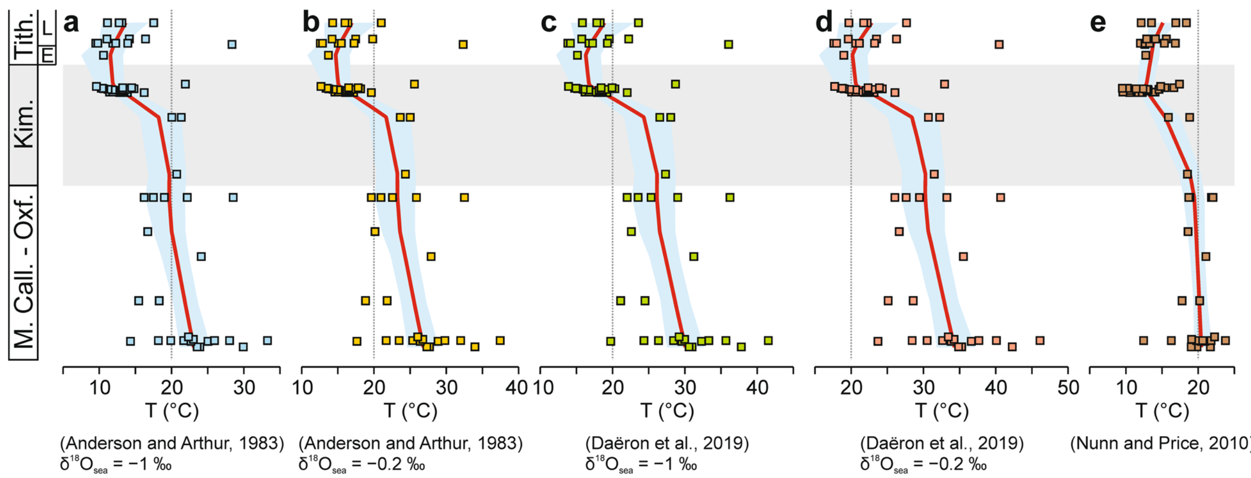

Fig. 10 Absolute temperature estimates for the Middle to Late Jurassic (Middle Callovian–Oxfordian, Kimmeridgian, Early and Late Tithonian) belemnite rostra of the Spiti Valley based on different methods. **a** Temperatures based on $\delta^{18}O_{shell}$ values, the equation of Anderson and Arthur (1983), and a $\delta^{18}O_{sea}$ value of – 1‰; **b** Temperatures based on $\delta^{18}O_{shell}$ values, the equation of Anderson and Arthur (1983), and a $\delta^{18}O_{sea}$ value of – 0.2‰; **c** Temperatures based on $\delta^{18}O_{shell}$ values, the equation of Daëron et al. (2019), and a $\delta^{18}O_{sea}$ value of – 1‰; **d** Temperatures based on $\delta^{18}O_{shell}$ values, the equation of Daëron et al. (2019), and a $\delta^{18}O_{sea}$ value of – 0.2‰; **e** Temperatures based on Mg/Ca values and the equation of Nunn and Price (2010)

(Zachos et al. 1994; Alberti et al. 2020a). Such a change would influence temperature reconstructions and increase the magnitude of the reconstructed cooling by around 1 °C.

Apart from temperature reconstructions based on $\delta^{18}O_{shell}$ values, the current dataset allows the application of the equation proposed by Nunn and Price (2010) on the measured Mg/Ca ratios (Fig. 10e). Since $\delta^{18}O_{shell}$ values and Mg/Ca ratios were found to show a strong negative correlation (Fig. 6b), it is not surprising that both proxies show similar trends. The temperature curve based on Mg/Ca ratios shows a very slight decrease in temperatures throughout the Middle Callovian–Oxfordian, which turns into a stronger cooling in the Kimmeridgian before again showing a slight temperature increase in the Tithonian. This development is also reflected in the average values (Table 3). Nevertheless, the reconstructed absolute temperature values are relatively low and comparable only to results from the equation of Anderson and Arthur (1983) at a $\delta^{18}O_{sea}$ value of −1‰. Consequently, this suggests that the equation of Nunn and Price (2010), which was developed based on data of benthic foraminifera (Lear et al. 2002), is not applicable for belemnite rostra. This potential problem was already noted by Nunn and Price (2010) and Price et al. (2018), but these authors suggested that at least the magnitude of temperature changes through time might be captured correctly. Following this reasoning, the present data suggest a temperature decrease from the Middle Callovian–Oxfordian to the Kimmeridgian/Tithonian by around 6 °C, which is almost identical to the temperature differences based on the maximum $\delta^{18}O_{shell}$ values mentioned above. The supposed drift of eastern Gondwana from 20°S to 30°S in the studied time interval would account for a cooling of around 5 °C or more assuming latitudinal temperature gradients similar to today (compare Alberti et al. 2019, 2020a).

In summary, it seems reliable to interpret the Middle to Late Jurassic $\delta^{18}O_{shell}$ and Mg/Ca record as reflecting a significant long-term cooling in the Himalayan study area by several degrees Celsius. While this temperature decrease seems to be strongest in the Kimmeridgian, the identification of further short-term fluctuations might be less reliable due to the scarcity of samples for some stratigraphic intervals and diagenetic alteration of some specimens in the tectonically highly active region. While the latter process complicates the reconstruction of absolute temperatures for the Middle Callovian–Oxfordian, it seems likely that the Kimmeridgian and Tithonian experienced water temperatures mostly between 17.6 °C and 27.6 °C (= 87% of all samples) with averages between 22 °C to 24 °C (compare Table 3). This way, average temperatures were largely comparable to or slightly higher than today's temperatures for the same latitudes (Shea et al. 1992), which fits in the general understanding of the Jurassic world (compare Alberti et al. 2020a). The scatter of around 10 °C in results from individual samples from the same stratigraphic intervals might either be caused by species-specific differences among the analysed belemnite taxa (e.g. different ecology) or short-term temperature fluctuations. Alternatively, it might represent a minimum estimate for seasonal temperature changes with some samples recording summer and some winter conditions.

6.4 Supra-regional comparisons

Reconstructions of absolute water temperatures for northeastern Gondwana in the Late Jurassic are still scarce, but the available data are comparable to the results from the Himalayas. Fürsich et al. (2005) proposed a climate change in the Kachchh Basin in western India from the Bathonian to the Oxfordian connected with a slight temperature decrease, more humid conditions, the disappearance of tropical taxa, and a change in sedimentology. This temperature decrease was later confirmed by Alberti et al. (2012a, 2012b) to continue until at least the Late Oxfordian. More recently, Alberti et al. (2019) reconstructed a long-term cooling of about 5 °C from the Callovian to the Oxfordian and Kimmeridgian for southern Madagascar based on stable oxygen isotope analyses of oyster shells. These authors suggested the concomitant rifting of Gondwana as the reason for the regional cooling, a view which is followed here. While eastern Gondwana drifted into higher latitudes, western Gondwana did not change its palaeogeographic position significantly (Fig. 8). Consequently, fossil material from northwestern Gondwana points to comparatively stable temperature conditions throughout the Middle and Late Jurassic as shown by Alberti et al. (2017, 2020a). Sadji et al. (2021) confirmed comparatively stable temperature conditions based on stable oxygen isotope analyses of belemnite rostra from Algeria with Oxfordian, Kimmeridgian, and Tithonian ages. These major long-term trends of northwestern and northeastern Gondwana might be modulated by short-term fluctuations caused by global climate changes, but these could not be identified for the mentioned study areas due to a scarcity of samples for some stratigraphic intervals and a commonly low biostratigraphic resolution.

In contrast to the Gondwanan data, a considerable number of stable oxygen isotope analyses from European localities compiled by Dera et al. (2011) and Martinez and Dera (2015) point to significant warming from the Late Callovian almost throughout the entire Late Jurassic. However, this European temperature increase might be overestimated as suggested by clumped isotope data, which point to more stable Late Jurassic temperatures with changing $\delta^{18}O_{sea}$ values instead (e.g. Wierzbowski et al. 2018; Vickers et al. 2020).

Considering absolute values, it might be worthwhile to note that the Kimmeridgian $\delta^{18}O_{shell}$ data of the present study from the southern hemisphere are very similar to results from the northern hemisphere at a comparable palaeolatitude (Wierzbowski 2015; Arabas 2016; Sadji et al. 2021).

7 Conclusions

Fossils collected from the Middle to Upper Jurassic succession of the Spiti and Zanskar valleys in the Indian Himalayas were analysed for their stable isotope ($\delta^{13}C$, $\delta^{18}O$) and element (Mg/Ca, Sr/Ca) composition. Cathodoluminescence and scanning electron microscopy in combination with the determination of iron and manganese contents were used to differentiate seemingly well from poorly preserved fossils. Consequently, all collected oyster shells as well as fossils from the Zanskar Valley had to be excluded from the interpretation as they showed strong signs of chemical alteration. Finally, 61 belemnite rostra from the Middle Callovian–Oxfordian, Kimmeridgian, and Tithonian of the Spiti Valley were used for temperature reconstructions. The results indicate a long-term temperature decrease of several degrees Celsius (around 5 °C or more), which can be connected to a synchronous drift of eastern Gondwana into higher latitudes. Absolute temperature estimates depend on the methodology, but based on the most recent research (Vickers et al. 2020), temperatures for belemnite $\delta^{18}O$ values were considered most realistic when calculated with the equation of Daëron et al. (2019) and a seawater $\delta^{18}O$ value of – 0.2‰. Following this approach, temperatures are proposed to vary mostly between 17.6 °C and 27.6 °C for the Kimmeridgian and Tithonian with average values being between 22 °C to 24 °C. Thereby, conditions would have been similar to slightly warmer than at comparable latitudes today. A relatively high number of poorly preserved specimens hinders the calculation of reliable absolute temperatures for the Middle Callovian –Oxfordian.

Acknowledgements

We thank Michael Joachimski and Birgit Leipner-Mata (Erlangen, Germany) for laboratory access. Karen Bremer and Verena Heinath (Kiel, Germany) helped with ICP-OES analyses. Birgit Mohr (Kiel, Germany) is thanked for support at the scanning electron microscope. We also thank the team of Hotel Deyzor (Kaza, India) for their outstanding hospitality during the field surveys. KSKV Kachchh University (Bhuj, India) is gratefully acknowledged for extending administrative support. The study was financially supported by the Alexander von Humboldt Foundation (Research Group Linkage Program), the German Research Foundation (DFG; Project AL 1740/3-1), the Strategic Priority Research Program of the Chinese Academy of Sciences (Grant No. XDB26000000), and the Second Tibetan Plateau Scientific Expedition and Research of the Ministry of Science and Technology of China (2019 QZKK0706). We thank Guillaume Dera, the anonymous reviewer, and the editors for their support and constructive comments.

Authors' contributions

All authors contributed in designing research and drafting of the manuscript. All authors read and approved the final manuscript.

Funding

The study was financially supported by the Alexander von Humboldt Foundation (Research Group Linkage Program), the German Research Foundation (DFG; Project AL 1740/3-1), the Strategic Priority Research Program of the Chinese Academy of Sciences (Grant No. XDB26000000), and the Second Tibetan Plateau Scientific Expedition and Research of the Ministry of Science and Technology of China (2019 QZKK0706).

Availability of data and materials

All data and relevant information are included in the published manuscript.

Declaration

Competing interests
The authors declare that they have no competing interests.

Author details
[1]State Key Laboratory for Mineral Deposits Research, School of Earth Sciences and Engineering, Centre for Research and Education on Biological Evolution and Environment and Frontiers Science Center for Critical Earth Material Cycling, Nanjing University, Nanjing 210023, Jiangsu Province, China. [2]GeoZentrum Nordbayern, Friedrich-Alexander-Universität Erlangen-Nürnberg, Loewenichstraße 28, 91054 Erlangen, Germany. [3]Department of Geology, School of Earth, Biological and Environmental Science, Central University of South Bihar SH 7, Gaya-Panchanpur Road, Village Karhara, Post Fatehpur, Gaya, Bihar 824236, India. [4]Department of Earth and Environmental Science, KSKV Kachchh University, Bhuj, India. [5]Leibniz Laboratory for Radiometric Dating and Stable Isotope Research, Christian-Albrechts-Universität zu Kiel, Max-Eyth-Straße 11, 24118 Kiel, Germany. [6]Institut für Geowissenschaften, Christian-Albrechts-Universität zu Kiel, Ludewig-Meyn-Straße 10, 24118 Kiel, Germany.

Received: 20 April 2021 Accepted: 22 July 2021
Published online: 30 August 2021

References

Ait-Itto, F.-Z., G.D. Price, A. Ait Addi, D. Chafiki, and I. Mannani. 2017. Bulk-carbonate and belemnite carbon-isotope records across the Pliensbachian–Toarcian boundary on the northern margin of Gondwana (Issouka, middle atlas, Morocco). *Palaeogeography, Palaeoclimatology, Palaeoecology* 466: 128–136. https://doi.org/10.1016/j.palaeo.2016.11.014.

Alberti, M., A. Agnieszka, F.T. Fürsich, N. Andersen, and P. Ziółkowski. 2019. The Middle to Upper Jurassic stable isotope record of Madagascar: Linking temperature changes with plate tectonics during the break-up of Gondwana. *Gondwana Research* 73: 1–15. https://doi.org/10.1016/j.gr.2019.03.012.

Alberti, M., F.T. Fürsich, A.A. Abdelhady, and N. Andersen. 2017. Middle to Late Jurassic equatorial seawater temperatures and latitudinal temperature gradients based on stable isotopes of brachiopods and oysters from Gebel Maghara, Egypt. *Palaeogeography, Palaeoclimatology, Palaeoecology* 468: 301–313. https://doi.org/10.1016/j.palaeo.2016.11.052.

Alberti, M., F.T. Fürsich, and D.K. Pandey. 2012a. The Oxfordian stable isotope record ($\delta^{18}O$, $\delta^{13}C$) of belemnites, brachiopods, and oysters from the Kachchh Basin (western India) and its potential for palaeoecologic, palaeoclimatic, and palaeogeographic reconstructions. *Palaeogeography, Palaeoclimatology, Palaeoecology* 344–345: 49–68.

Alberti, M., F.T. Fürsich, D.K. Pandey, and M. Ramkumar. 2012b. Stable isotope analyses of belemnites from the Kachchh Basin, western India: Paleoclimatic implications for the Middle to Late Jurassic transition. *Facies* 58 (2): 261–278. https://doi.org/10.1007/s10347-011-0278-9.

Alberti, M., Y. Leshno, F.T. Fürsich, Y. Edelman-Furstenberg, N. Andersen, and D. Garbe-Schönberg. 2020a. Stress in the tropics? Impact of a latitudinal seawater $\delta^{18}O$ gradient on Middle Jurassic temperature reconstructions at low latitudes. *Geology* 48 (12): 1210–1215. https://doi.org/10.1130/G47824.1.

Alberti, M., D.K. Pandey, M. Hethke, and F.T. Fürsich. 2015. Ammonites of the subfamily Mayaitinae Spath, 1928 from the Oxfordian of Kachchh, Western India. *Geobios* 48 (2): 85–130. https://doi.org/10.1016/j.geobios.2015.02.005.

Alberti, M., H. Parent, A.C. Garrido, N. Andersen, D. Garbe-Schönberg, and S. Danise. 2020b. Stable isotopes ($\delta^{13}C$, $\delta^{18}O$) and element ratios (Mg/Ca, Sr/Ca) of Jurassic belemnites, bivalves and brachiopods from the Neuquén Basin (Argentina): Challenges and opportunities for palaeoenvironmental reconstructions. *Journal of the Geological Society, London* 178: jgs2020–jgs2163.

Anderson, T.F., and M.A. Arthur. 1983. Stable isotopes of oxygen and carbon and their application to sedimentological and paleoenvironmental problems. In *Stable isotopes in sedimentary geology. SEPM Short Course*, ed. M.A. Arthur, T.F. Anderson, I.R. Kaplan, J. Veizer, and L. Land, vol. 10, 1–151.

Arabas, A. 2016. Middle–Upper Jurassic stable isotope records and seawater temperature variations: New palaeoclimate data from marine carbonate and belemnite rostra (Pieniny Klippen Belt, Carpathians). *Palaeogeography, Palaeoclimatology, Palaeoecology* 446: 284–294. https://doi.org/10.1016/j.palaeo.2016.01.033.

Arabas, A., J. Schlögel, and C. Meister. 2017. Early Jurassic carbon and oxygen isotope records and seawater temperature variations: Insights from marine carbonate and belemnite rostra (Pieniny Klippen Belt, Carpathians). *Palaeogeography, Palaeoclimatology, Palaeoecology* 485: 119–135. https://doi.org/10.1016/j.palaeo.2017.06.007.

Bailey, T.R., Y. Rosenthal, J.M. McArthur, B. van de Schootbrugge, and M.F. Thirlwall. 2003. Paleoceanographic changes of the late Pliensbachian–early Toarcian interval: A possible link to the genesis of an oceanic anoxic event. *Earth and Planetary Science Letters* 212 (3-4): 307–320. https://doi.org/10.1016/S0012-821X(03)00278-4.

Bajnai, D., J. Fiebig, A. Tomašových, S. Milner Garcia, C. Rollion-Bard, J. Raddatz, N. Löffler, C. Primo-Ramos, and U. Brand. 2018. Assessing kinetic fractionation in brachiopod calcite using clumped isotopes. *Scientific Reports* 8 (1): 533. https://doi.org/10.1038/s41598-017-17353-7.

Baud, A., M. Gaetani, E. Garzanti, E. Fois, A. Nicora, and A. Tintori. 1984. Geological observations in southeastern Zanskar and adjacent Lahul area (northwestern Himalaya). *Eclogae Geologicae Helvetiae* 77: 171–197.

Bertle, R.J., and T.J. Suttner. 2005. New biostratigraphic data for the Chikkim Formation (Cretaceous, Tethya Himalaya, India). *Cretaceous Research* 26 (6): 882–894. https://doi.org/10.1016/j.cretres.2005.06.001.

Bertle, R.J., and T.J. Suttner. 2021. Facies, sequence stratigraphy and depositional environment of the Lower Cretaceous Giumal Formation in Spiti (Tethyan Himalaya, India). *Marine and Petroleum Geology* 128: 105009. https://doi.org/10.1016/j.marpetgeo.2021.105009.

Besse, J., and V. Courtillot. 2002. Apparent and true polar wander and the geometry of the geomagnetic field over the last 200 Myr. *Journal of Geophysical Research* 107: 2300.

Bhargava, O.N. 2008. An updated introduction to the Spiti geology. *Journal of the Palaeontological Society of India* 53: 113–129.

Bhargava, O.N., and U.K. Bassi. 1998. Geology of Spiti-Kinnaur Himachal Himalaya. *Memoirs of the Geological Survey of India* 124: 1–210.

Blanford, H.F. 1864. On Dr. Gerard's collection of fossils from the Spiti Valley, in the Asiatic Society's Museum. *Journal of the Asiatic Society of Bengal* 32: 124–138.

Bougeois, L., M. de Rafélis, G.-J. Reichart, L.J. de Nooijer, and G. Dupont-Nivet. 2016. Mg/Ca in fossil oyster shells as palaeotemperature proxy, an example from the Palaeogene of Central Asia. *Palaeogeography, Palaeoclimatology, Palaeoecology* 441: 611–626. https://doi.org/10.1016/j.palaeo.2015.09.052.

Bowen, R. 1963. O^{18}/O^{16} paleotemperature measurements on Mesozoic Belemnoidea from Neuquen and Santa Cruz provinces, Argentina. *Journal of Paleontology* 37: 714–718.

Brand, U., and J. Veizer. 1980. Chemical diagenesis of a multicomponent carbonate system — 1: Trace elements. *Journal of Sedimentary Petrology* 50: 1219–1236.

Brand, U., and J. Veizer. 1981. Chemical diagenesis of a multicomponent carbonate system — 2: Stable isotopes. *Journal of Sedimentary Petrology* 51: 987–997.

Brookfield, M.E., and G.E.G. Westermann. 1982. Mesozoic ammonites from the Spong Valley, Zanskar, N.W. India. *Journal of the Geological Society of India* 23: 263–266.

Cariou, E., and R. Enay. 1999. Les ammonites du Bathonien et du Callovien de Thakkhola (Népal Central): Biochronologie et intérêt paléobiogéographique. *Geobios* 32 (5): 701–726. https://doi.org/10.1016/S0016-6995(99)80058-8.

Cariou, E., R. Enay, and Y. Almeras. 1996. Découverte d'une faune d'ammonites callovienne dans les Spiti Shales himalayens à Spiti et chronostratigraphie comparée des successions du Jurassique moyen et supérieur de Spiti et du Népal central (Thakkhola). *Comptes Rendus de l'Académie des Sciences* 322: 861–868.

Cléroux, C., E. Cortijo, P. Anand, L. Labeyrie, F. Bassinot, N. Caillon, and J.-C. Duplessy. 2008. Mg/Ca and Sr/Ca ratio in planktonic foraminifera: Proxies for upper water column temperature reconstruction. *Paleoceanography* 23: PA3214.

Coplen, T.B. 2007. Calibration of the calcite–water oxygen-isotope geothermometer at devils hole, Nevada, a natural laboratory. *Geochimica et Cosmochimica Acta* 71 (16): 3948–3957. https://doi.org/10.1016/j.gca.2007.05.028.

Craig, H. 1965. The measurement of oxygen isotope paleotemperatures. In *Stable isotopes in oceanographic studies and paleotemperatures. Consiglio Nazionale delle Ricerche Laboratorio di Geologia Nucleare, Pisa*, ed. E. Tongiorgi, 161–182.

Daëron, M., R.N. Drydale, M. Peral, D. Huyghe, D. Blamart, T.B. Coplen, F. Lartaud, and G. Zanchetta. 2019. Most earth-surface calcites precipitate out of isotopic equilibrium. *Nature Communications* 10 (1): 429. https://doi.org/10.1038/s41467-019-08336-5.

Danise, S., G.D. Price, M. Alberti, and S.M. Holland. 2020. Isotopic evidence for partial geochemical decoupling between a Jurassic epicontinental sea and the open ocean. *Gondwana Research* 82: 97–107. https://doi.org/10.1016/j.gr.2019.12.011.

Davies, A.J., S. Davis, and C.M. John. 2021. Evidence of taxonomic non-equilibrium effects in the clumped isotope composition of modern cephalopod carbonate. *Chemical Geology* 578: 120317. https://doi.org/10.1016/j.chemgeo.2021.120317.

Dera, G., B. Brigaud, F. Monna, R. Laffont, E. Pucéat, J.-F. Deconinck, P. Pellenard, M.M. Joachimski, and C. Durlet. 2011. Climatic ups and downs in a disturbed Jurassic world. *Geology* 39 (3): 215–218. https://doi.org/10.1130/G31579.1.

Eggins, S., P. Deckker, and J. Marshall. 2003. Mg/Ca variation in planktonic foraminifera tests: Implications for reconstructing palaeo-seawater temperature and habitat migration. *Earth and Planetary Science Letters* 212 (3-4): 291–306. https://doi.org/10.1016/S0012-821X(03)00283-8.

Enay, R. 2009. Les faunes d'ammonites de l'Oxfordien au Tithonien et la biostratigraphie des Spiti-Shales (Callovien supérieur–Tithonien) de Thakkhola, Népal Central. *Documents des Laboratoires de Géologie Lyon* 166: 1–351.

Enay, R., and E. Cariou. 1997. Ammonite faunas and palaeobiogeography of the Himalayan belt during the Jurassic: Initiation of a Late Jurassic austral ammonite fauna. *Palaeogeography, Palaeoclimatology, Palaeoecology* 134 (1-4): 1–38. https://doi.org/10.1016/S0031-0182(96)00157-5.

Epstein, S., R. Buchsbaum, and H.A. Lowenstam. 1953. Revised carbonate-water isotopic temperature scale. *Geological Society of America Bulletin* 64 (11): 1315–1325. https://doi.org/10.1130/0016-7606(1953)64[1315:RCITS]2.0.CO;2.

Epstein, S., R. Buchsbaum, H.A. Lowenstam, and H.C. Urey. 1951. Carbonate-water isotopic temperature scale. *Geological Society of America Bulletin* 62 (4): 417–426. https://doi.org/10.1130/0016-7606(1951)62[417:CITS]2.0.CO;2.

Fernandez, A., C. Korte, C.V. Ullmann, N. Looser, S. Wohlwend, and S.M. Bernasconi. 2021. Reconstructing the magnitude of early Toarcian (Jurassic) warming using the reordered clumped isotope compositions of belemnites. *Geochimica et Cosmochimica Acta* 293: 308–327. https://doi.org/10.1016/j.gca.2020.10.005.

Fürsich, F.T., I.B. Singh, M. Joachimski, S. Krumm, M. Schlirf, and S. Schlirf. 2005. Palaeoclimatic reconstructions of the Middle Jurassic of Kachchh (western India): An integrated approach based on palaeoecological, oxygen isotopic, and clay mineralogical data. *Palaeogeography, Palaeoclimatology, Palaeoecology* 217 (3-4): 289–309. https://doi.org/10.1016/j.palaeo.2004.11.026 .

Gaetani, M., R. Casnedi, E. Fois, E. Garzanti, F. Jadoul, A. Nicora, and A. Tintori. 1986. Stratigraphy of the Tethys Himalaya in Zanskar, Ladakh — Initial report. *Rivista Italiana di Paleontologia e Stratigrafia* 91: 443–478.

Garzanti, E., F. Jadoul, A. Nicora, and F. Berra. 1995. Triassic of Spiti (Tethys Himalaya, N India). *Rivista Italiana di Paleontologia e Stratigrafia* 101: 267–300.

Greaves, M., N. Caillon, H. Rebaubier, G. Bartoli, S. Bohaty, I. Cacho, L. Clarke, M. Cooper, C. Daunt, M. Delaney, P. deMenocal, A. Dutton, S. Eggins, H. Elderfield, D. Garbe-Schoenberg, E. Goddard, D. Green, J. Groeneveld, D. Hastings, E. Hathorne, K. Kimoto, G. Klinkhammer, L. Labeyrie, D.W. Lea, T. Marchitto, M.A. Martínez-Botí, P.G. Mortyn, Y. Ni, D. Nuernberg, G. Paradis, L. Pena, T. Quinn, Y. Rosenthal, A. Russell, T. Sagawa, S. Sosdian, L. Stott, K. Tachikawa, E. Tappa, R. Thunell, and P.A. Wilson. 2008. Interlaboratory comparison study of calibration standards for foraminiferal Mg/Ca thermometry. *Geochemistry, Geophysics, Geosystems* 9: Q08010.

Gupta, V.J., and S. Kumar. 1975. Geology of Ladakh, Lahaul and Spiti regions of Himalaya with special reference to the stratigraphic position of flysch deposits. *Geologische Rundschau* 64 (1): 540–563. https://doi.org/10.1007/BF01820682.

Hathorne, E.C., A. Gagnon, T. Felis, J. Adkins, R. Asami, W. Boer, N. Caillon, D. Case, K.M. Cobb, E. Douville, P. deMenocal, A. Eisenhauer, D. Garbe-Schönberg, W. Geibert, S. Goldstein, K. Hughen, M. Inoue, H. Kawahata, M. Kölling, F.L. Cornec, B.K. Linsley, H.V. McGregor, P. Montagna, I.S. Nurhati, T.M. Quinn, J. Raddatz, H. Rebaubier, L. Robinson, A. Sadekov, R. Sherrell, D. Sinclair, A.W. Tudhope, G. Wei, H. Wong, H.C. Wu, and C.-F. You. 2013. Interlaboratory study for coral Sr/Ca and other element/Ca ratio measurements. *Geochemistry, Geophysics, Geosystems* 14 (9): 3730–3750. https://doi.org/10.1002/ggge.20230.

Hodgson, W.A. 1966. Carbon and oxygen isotope ratios in diagenetic carbonates from marine sediments. *Geochimica et Cosmochimica Acta* 30 (12): 1223–1233. https://doi.org/10.1016/0016-7037(66)90121-9.

Hoffmann, R., and K. Stevens. 2019. The palaeobiology of belemnites — Foundation for the interpretation of rostrum geochemistry. *Biological Reviews* 95: 94–123.

Holdhaus, K. 1912. Fauna of the Spiti Shales (Lamellibranchiata and Gastropoda). In *Memoirs of the geological survey of India, Palaeontologia Indica Series 15, 5, Part 2, Fasc. No. 4*, 397–456.

Hudson, J.D. 1977. Stable isotopes and limestone lithification. *Journal of the Geological Society, London* 133 (6): 637–660. https://doi.org/10.1144/gsjgs.133.6.0637.

Jadoul, F., E. Fois, A. Tintori, and E. Garzanti. 1985. Preliminary results on Jurassic stratigraphy in Zanskar (NW Himalaya). *Rendiconti Società Geologica Italiana* 8: 9–13.

Jadoul, F., E. Garzanti, and E. Fois. 1990. Upper Triassic–Lower Jurassic stratigraphy and paleogeographic evolution of the Zanskar Tethys Himalaya (Zangla Unit). *Rivista Italiana di Paleontologia e Stratigrafia* 95: 351–396.

Jain, K.P., R. Garg, S. Kumar, and I.B. Singh. 1984. Upper Jurassic dinoflagellate biostratigraphy of Spiti shale (formation), Malla Johar area, Tethys Himalaya, India. *Journal of the Palaeontological Society of India* 29: 67–83.

Jochum, K.P., U. Nohl, K. Herwig, E. Lammel, B. Stoll, and A.W. Hofmann. 2007. GeoReM: A new geochemical database for reference materials and isotopic standards. *Geostandards and Geoanalytical Research* 29: 333–338.

Kele, S., S.F.M. Breitenbach, E. Capezzuoli, A.N. Meckler, M. Ziegler, I.M. Millan, T. Kluge, J. Deák, K. Hanselmann, C.M. John, H. Yan, Z. Liu, and S.M. Bernasconi. 2015. Temperature dependence of oxygen- and clumped isotope fractionation in carbonates: A study of travertines and tufas in the 6–95°C temperature range. *Geochimica et Cosmochimica Acta* 168: 172–192. https://doi.org/10.1016/j.gca.2015.06.032.

Kent, D.V., and E. Irving. 2010. Influence of inclination error in sedimentary rocks on the Triassic and Jurassic apparent pole wander path for North America and implications for cordilleran tectonics. *Journal of Geophysical Research* 115 (B10): B10103. https://doi.org/10.1029/2009JB007205.

Kim, S.-T., and J.R. O'Neil. 1997. Equilibrium and nonequilibrium oxygen isotope effects in synthetic carbonates. *Geochimica et Cosmochimica Acta* 61 (16): 3461–3475. https://doi.org/10.1016/S0016-7037(97)00169-5.

Korte, C., S.P. Hesselbo, C.V. Ullmann, G. Dietl, M. Ruhl, G. Schweigert, and N. Thibault. 2015. Jurassic climate mode governed by ocean gateway. *Nature Communications* 6 (1): 10015. https://doi.org/10.1038/ncomms10015.

Krishna, J. 1983. Callovian–Albian ammonoid stratigraphy and palaeobiogeography in the Indian sub-continent with special reference to the Tethys Himalaya. *Himalayan Geology* 11: 43–72.

Krishna, J., S. Kumar, and I.B. Singh. 1982. Ammonoid stratigraphy of the Spiti shale (Upper Jurassic), Tethys Himalaya, India. *Neues Jahrbuch für Geologie und Paläontologie, Monatshefte* 1982 (10): 580–592. https://doi.org/10.1127/njgpm/1982/1982/580.

Lear, C.H., Y. Rosenthal, and N. Slowey. 2002. Benthic foraminiferal Mg/Ca-paleothermometry: A revised core-top calibration. *Geochimica et Cosmochimica Acta* 66 (19): 3375–3387. https://doi.org/10.1016/S0016-7037(02)00941-9.

LeGrande, A.N., and G.A. Schmidt. 2006. Global gridded data set of the oxygen isotopic composition in seawater. *Geophysical Research Letters* 33 (12): L12604. https://doi.org/10.1029/2006GL026011.

Leng, M.J., and J.D. Marshall. 2004. Palaeoclimate interpretation of stable isotope data from lake sediment archives. *Quaternary Science Reviews* 23 (7-8): 811–831. https://doi.org/10.1016/j.quascirev.2003.06.012.

Li, Q., J.M. McArthur, P. Doyle, N. Janssen, M.J. Leng, W. Müller, and S. Reboulet. 2013. Evaluating Mg/Ca in belemnite calcite as a palaeo-proxy. *Palaeogeography, Palaeoclimatology, Palaeoecology* 388: 98–108.

Lukeneder, A., T.J. Suttner, and R.J. Bertle. 2013. New ammonoid taxa from the Lower Cretaceous Giumal Formation of the Tethyan Himalaya (northern India). *Palaeontology* 56 (5): 991–1028. https://doi.org/10.1111/pala.12032.

Marshall, J.D. 1992. Climatic and oceanographic isotopic signals from the carbonate rock record and their preservation. *Geological Magazine* 129 (2): 143–160. https://doi.org/10.1017/S0016756800008244.

Martinez, M., and G. Dera. 2015. Orbital pacing of carbon fluxes by a ~9-my eccentricity cycle during the Mesozoic. *Proceedings of the National Academy of Sciences* 112 (41): 12604–12609. https://doi.org/10.1073/pnas.1419946112.

McArthur, J.M., P. Doyle, M.J. Leng, K. Reeves, C.T. Williams, R. Garcia-Sanchez, and R.J. Howarth. 2007. Testing palaeo-environmental proxies in Jurassic belemnites: Mg/Ca, Sr/Ca, Na/Ca, $\delta^{18}O$ and $\delta^{13}C$. *Palaeogeography, Palaeoclimatology, Palaeoecology* 252 (3-4): 464–480. https://doi.org/10.1016/j.palaeo.2007.05.006.

Mouchi, V., M. de Rafélis, F. Lartaud, M. Fialin, and E. Verrecchia. 2013. Chemical labelling of oyster shells used for time-calibrated high-resolution Mg/Ca ratios: A tool for estimation of past seasonal temperature variations. *Palaeogeography, Palaeoclimatology, Palaeoecology* 373: 66–74. https://doi.org/10.1016/j.palaeo.2012.05.023.

Mutterlose, J., M. Malkoc, S. Schouten, J.S. Sinninghe Damsté, and A. Forster. 2010. TEX_{86} and stable $\delta^{18}O$ paleothermometry of Early Cretaceous sediments: Implications for belemnite ecology and paleotemperature proxy applications. *Earth and Planetary Science Letters* 298 (3-4): 286–298. https://doi.org/10.1016/j.epsl.2010.07.043.

Nelson, C.S., and A.M. Smith. 1996. Stable oxygen and carbon isotope compositional fields for skeletal and diagenetic components in New Zealand Cenozoic nontropical carbonate sediments and limestones: A synthesis and review. *New Zealand Journal of Geology and Geophysics* 39 (1): 93–107. https://doi.org/10.1080/00288306.1996.9514697.

Nunn, E.V., and G.D. Price. 2010. Late Jurassic (Kimmeridgian–Tithonian) stable isotopes ($\delta^{18}O$, $\delta^{13}C$) and Mg/Ca ratios: New palaeoclimatic data from Helmsdale, Northeast Scotland. *Palaeogeography, Palaeoclimatology, Palaeoecology* 292 (1-2): 325–335. https://doi.org/10.1016/j.palaeo.2010.04.015.

Oloriz, F., and A. Tintori. 1991. Upper Jurassic (Tithonian) ammonites from the Spiti Shales in western Zanskar (NW Himalayas). *Rivista Italiana di Paleontologia e Stratigrafia* 96: 461–486.

O'Neil, J.R., R.N. Clayton, and T.K. Mayeda. 1969. Oxygen isotope fractionation in divalent metal carbonates. *Journal of Chemical Physics* 51 (12): 5547–5558. https://doi.org/10.1063/1.1671982.

Pandey, B., D.B. Pathak, and J. Krishna. 2013. Preliminary remarks on new ammonoid collection from freshly exposed succession of the Spiti Formation between Lidang and Giumal, Spiti Valley, Himachal Himalaya, India. *Himalayan Geology* 34: 124–134.

Pathak, D.B. 1993. The first record of the ammonite genus *Hybonoticeras* from the Himalaya and its biostratigraphic significance. *Newsletters on Stratigraphy* 28 (2-3): 121–129. https://doi.org/10.1127/nos/28/1993/121.

Pathak, D.B. 1997. Ammonoid stratigraphy of the Spiti shale formation in Spiti Himalaya, India. *Journal of the Geological Society of India* 50: 191–200.

Pathak, D.B. 2007. Jurassic/Cretaceous boundary in the Spiti Himalaya, India. *Journal of Palaeontological Society of India* 52: 51–57.

Price, G.D., D. Bajnai, and J. Fiebig. 2020. Carbonate clumped isotope evidence for latitudinal seawater temperature gradients and the oxygen isotope composition of Early Cretaceous seas. *Palaeogeography, Palaeoclimatology, Palaeoecology* 552: 109777. https://doi.org/10.1016/j.palaeo.2020.109777.

Price, G.D., M.B. Hart, P.R. Wilby, and K.N. Page. 2015. Isotopic analysis of Jurassic (Callovian) mollusks from the Christian Malford Lagerstätte (UK): Implications for ocean water temperature estimates based on belemnoids. *Palaios* 30 (9): 645–654. https://doi.org/10.2110/palo.2014.106.

Price, G.D., N.M.M. Janssen, M. Martinez, M. Company, J.H. Vandevelde, and S.T. Grimes. 2018. A high-resolution belemnite geochemical analysis of Early Cretaceous (Valanginian–Hauterivian) environmental and climatic perturbations. *Geochemistry, Geophysics, Geosystems* 19: 3832–3843.

Price, G.D., and B.W. Sellwood. 1997. "Warm" palaeotemperatures from high Late Jurassic palaeolatitudes (Falkland plateau): Ecological, environmental or diagenetic controls? *Palaeogeography, Palaeoclimatology, Palaeoecology* 129 (3-4): 315–327. https://doi.org/10.1016/S0031-0182(96)00058-2.

Prokoph, A., G.A. Shields, and J. Veizer. 2008. Compilation and time-series analysis of a marine carbonate $\delta^{18}O$, $\delta^{13}C$, $^{87}Sr/^{86}Sr$ and $\delta^{34}S$ database through Earth history. *Earth-Science Reviews* 87 (3-4): 113–133. https://doi.org/10.1016/j.earscirev.2007.12.003.

Roche, D.M., Y. Donnadieu, E. Pucéat, and D. Paillard. 2006. Effect of changes in $\delta^{18}O$ content of the surface ocean on estimated sea surface temperatures in past warm climate. *Paleoceanography* 21: PA2023.

Sadji, R., A. Munnecke, M. Benhamou, M. Alberti, S. Belkhedim, and N. Ramdane. 2021. Late Jurassic temperatures for the southern Tethyan margin based on belemnites $\delta^{18}O$ from the Ouarsenis Mountains, northwestern Algeria. *Palaeogeography, Palaeoclimatology, Palaeoecology* 566: 110224. https://doi.org/10.1016/j.palaeo.2021.110224.

Shackleton, N.J., and J.P. Kennett. 1975. Paleotemperature history of the Cenozoic and the initiation of Antarctic glaciation: Oxygen and carbon isotope analyses in DSDP sites 277, 279, and 281. *Initial Reports of the Deep Sea Drilling Project* 29: 743–755.

Shea, D.J., K.E. Trenberth, and R.W. Reynolds. 1992. A global monthly sea surface temperature climatology. *Journal of Climate* 5 (9): 987–1001. https://doi.org/10.1175/1520-0442(1992)0050987:AGMSST2.0.CO;2.

Steuber, T., and J. Veizer. 2002. Phanerozoic record of plate tectonic control of seawater chemistry and carbonate sedimentation. *Geology* 30 (12): 1123–1126. https://doi.org/10.1130/0091-7613(2002)030<1123:PROPTC>2.0.CO;2.

Stevens, G.R., and R.N. Clayton. 1971. Oxygen isotope studies on Jurassic and Cretaceous belemnites from New Zealand and their biogeographic significance. *New Zealand Journal of Geology and Geophysics* 14 (4): 829–897. https://doi.org/10.1080/00288306.1971.10426336 .

Stoliczka, F. 1865. Geological sections across the Himalayan Mountains from Wangtu bridge on the river Sutlej to Sungdo on the Indus, with an account of the formations in Spiti, accompanied by a revision of all known fossils from that district. *Memoirs of the Geological Survey of India* 5: 1–152.

Surge, D., and K. Lohmann. 2008. Evaluating Mg/Ca ratios as a temperature proxy in the estuarine oyster, *Crassostrea virginica*. *Journal of Geophysical Research* 113: G02001.

Takayanagi, H., R. Asami, O. Abe, T. Miyajima, H. Kitagawa, K. Sasaki, and Y. Iryu. 2013. Intraspecific variations in carbon-isotope and oxygen-isotope compositions of a brachiopod *Basiliola lucida* collected off Okinawa-jima, southwestern Japan. *Geochimica et Cosmochimica Acta* 115: 115–136. https://doi.org/10.1016/j.gca.2013.03.026.

Tiwari, R.S., V.D.M. Vijaya, and R.S. Misra. 1996. Palynological studies on a Late Palaeozoic–Mesozoic Tethyan sequence in the Niti area of the Central Himalaya, Uttar Pradesh, India. *Review of Palaeobotany and Palynology* 94 (1-2): 169–196. https://doi.org/10.1016/0034-6667(95)00112-3.

Torsvik, T.H., R. van der Voo, U. Preeden, C. MacNiocaill, B. Steinberger, P.V. Doubrovine, D.J.J. van Hinsbergen, M. Domeier, C. Gaina, E. Tohver, J.G. Meert, P.J.A. McCausland, and L.R.M. Cocks. 2012. Phanerozoic polar wander, palaeogeography and dynamics. *Earth-Science Reviews* 114 (3-4): 325–368. https://doi.org/10.1016/j.earscirev.2012.06.007.

Tynan, S., B.N. Opdyke, M. Walczak, S. Eggins, and A. Dutton. 2017. Assessment of Mg/Ca in *Saccostrea glomerata* (the Sydney rock oyster) shell as a potential temperature record. *Palaeogeography, Palaeoclimatology, Palaeoecology* 484: 79–88. https://doi.org/10.1016/j.palaeo.2016.08.009.

Uhlig, V. 1903. The fauna of the Spiti shales. *Memoirs of the Geological Survey of India, Series 15* 4: 1–132.

Ullmann, C.V., H.J. Campbell, R. Frei, and C. Korte. 2016. Oxygen and carbon isotope and Sr/Ca signature of high-latitude Permian to Jurassic calcite fossils from New Zealand and New Caledonia. *Gondwana Research* 38: 60–73. https://doi.org/10.1016/j.gr.2015.10.010.

Ullmann, C.V., S.P. Hesselbo, and C. Korte. 2013. Tectonic forcing of Early to Middle Jurassic seawater Sr/Ca. *Geology* 41 (12): 1211–1214. https://doi.org/10.1130/G34817.1.

Ullmann, C.V., and C. Korte. 2015. Diagenetic alteration in low-Mg calcite from macrofossils: A review. *Geological Quarterly* 59: 3–20.

Urey, H.C., H.A. Lowenstam, S. Epstein, and C.R. McKinney. 1951. Measurement of paleotemperatures and temperatures of the Upper Cretaceous of England, Denmark, and the southeastern United States. *Geological Society of America Bulletin* 62 (4): 399–416. https://doi.org/10.1130/0016-7606(1951)62[399:MOPATO]2.0.CO;2.

van Hinsbergen, D.J.J., L.V. de Groot, S.J. van Schalk, W. Spakman, P.K. Bijl, A. Sluijs, C.G. Langereis, and H. Brinkhuis. 2015. A paleolatitude calculator for paleoclimate studies. *PLoS One* 10 (6): e0126946. https://doi.org/10.1371/journal.pone.0126946.

Vickers, M.L., A. Fernandez, S.P. Hesselbo, G.D. Price, S.M. Bernasconi, S. Lode, C.V. Ullmann, N. Thibault, I.W. Hougaard, and C. Korte. 2020. Unravelling Middle to Late Jurassic palaeoceanographic and palaeoclimatic signals in the Hebrides Basin using belemnite clumped isotope thermometry. *Earth and Planetary Science Letters* 546: 116401. https://doi.org/10.1016/j.epsl.2020.116401.

Vijaya, S.K. 2002. Palynostratigraphy of the Spiti shale (Oxfordian–Berriasian) of Kumaon Tethys Himalaya, Malla Johar area, India. *Review of Palaeobotany and Palynology* 122 (3-4): 143–153. https://doi.org/10.1016/S0034-6667(02)00116-1.

Wierzbowski, H. 2002. Detailed oxygen and carbon isotope stratigraphy of the Oxfordian in Central Poland. *International Journal of Earth Sciences* 91 (2): 304–314. https://doi.org/10.1007/s005310100217.

Wierzbowski, H. 2004. Carbon and oxygen isotope composition of Oxfordian–early Kimmeridgian belemnite rostra: Palaeoenvironmental implications for Late Jurassic seas. *Palaeogeography, Palaeoclimatology, Palaeoecology* 203 (1-2): 153–168. https://doi.org/10.1016/S0031-0182(03)00673-4.

Wierzbowski, H. 2015. Seawater temperatures and carbon isotope variations in central European basins at the Middle–Late Jurassic transition (late Callovian–early Kimmeridgian). *Palaeogeography, Palaeoclimatology, Palaeoecology* 440: 506–523. https://doi.org/10.1016/j.palaeo.2015.09.020.

Wierzbowski, H., D. Bajnai, U. Wacker, M.A. Rogov, J. Fiebig, and E.M. Tesakova. 2018. Clumped isotope record of salinity variations in the Subboreal Province at the Middle–Late Jurassic transition. *Global and Planetary Change* 167: 172–189. https://doi.org/10.1016/j.gloplacha.2018.05.014.

Wierzbowski, H., K. Dembicz, and T. Praszkier. 2009. Oxygen and carbon isotope composition of Callovian–Lower Oxfordian (Middle–Upper Jurassic) belemnite rostra from central Poland: A record of a late Callovian global sea-level rise? *Palaeogeography, Palaeoclimatology, Palaeoecology* 283 (3-4): 182–194. https://doi.org/10.1016/j.palaeo.2009.09.020.

Wierzbowski, H., and M. Joachimski. 2007. Reconstruction of late Bajocian–Bathonian marine palaeoenvironments using carbon and oxygen isotope ratios of calcareous fossils from the Polish Jura Chain (Central Poland). *Palaeogeography, Palaeoclimatology, Palaeoecology* 254 (3-4): 523–540. https://doi.org/10.1016/j.palaeo.2007.07.010 .

Zachos, J.C., L.D. Stott, and K.C. Lohmann. 1994. Evolution of Early Cenozoic marine temperatures. *Palaeoceanography* 9 (2): 353–387. https://doi.org/10.1029/93PA03266.

Publisher's Note

Springer Nature remains neutral with regard to jurisdictional claims in published maps and institutional affiliations.

Submit your manuscript to a SpringerOpen journal and benefit from:

► Convenient online submission
► Rigorous peer review
► Open access: articles freely available online
► High visibility within the field
► Retaining the copyright to your article

Submit your next manuscript at ► springeropen.com